Available online at www.sciencedirect.com
ScienceDirect
Journal of Sound and Vibration 321 (2009) 375–404
JOURNAL OF SOUND AND VIBRATION
www.elsevier.com/locate/jsvi

A spectral-Tchebychev technique for solving linear and nonlinear beam equations

Baris Yagci[a], Sinan Filiz[a], Louis L. Romero[b], O. Burak Ozdoganlar[a,*]

[a]*Department of Mechanical Engineering, Carnegie Mellon University, Pittsburgh, PA 15213, USA*
[b]*Sandia National Laboratories, Albuquerque, NM 87185, USA*

Received 26 April 2007; received in revised form 22 July 2008; accepted 15 September 2008
Handling Editor: S. Bolton
Available online 25 November 2008

Abstract

This paper presents a spectral-Tchebychev technique for solving linear and nonlinear beam problems. The technique uses Tchebychev polynomials as spatial basis functions, and applies Galerkin's method to obtain the spatially discretized equations of motion. Unlike alternative techniques that require different admissible functions for each different set of boundary conditions, the spectral-Tchebychev technique incorporates the boundary conditions into the derivation, and thereby enables the utilization of the solution for any linear boundary conditions without re-derivation. Furthermore, the proposed technique produces symmetric system matrices for self-adjoint problems. In this work, the spectral-Tchebychev solutions for Euler–Bernoulli and Timoshenko beams are derived. The convergence and accuracy characteristics of the spectral-Tchebychev technique is studied by solving eigenvalue problems with different boundary conditions. It is found that the convergence is exponential, and a small number of polynomials is sufficient to obtain machine-precision accuracy. The application of the technique is demonstrated by solving: (1) eigenvalue problems for tapered Timoshenko beams with different boundary conditions, taper ratios, and beam lengths; (2) an Euler–Bernoulli beam problem with spatially and temporally varying forcing, elastic boundary, and damping; (3) large-deflection (nonlinear) Euler–Bernoulli beam problems with different boundary conditions; and (4) a micro-beam problem with nonlinear electrostatic excitation. The results obtained from the spectral-Tchebychev solutions are seen to be in excellent agreement with those presented in the literature.

1. Introduction

In the presence of nonuniform parameters and complicated boundary conditions, the spectral–temporal boundary-value problems that describe the distributed-parameter models of beam dynamics do not lend themselves to closed-form analytical solutions. Therefore, a wide range of approximate solutions have been derived to solve beam problems. Approximate solutions include approaches for discretization of the spatial part of the problem. A commonly used method for spatial discretization is to describe the spatial dependence with an assumed solution in a series form with known functions. The use of the assumed solutions in

*Corresponding author. Tel.: +1 412 2689890.
E-mail address: ozdoganlar@cmu.edu (O.B. Ozdoganlar).

0022-460X/$ - see front matter © 2008 Elsevier Ltd. All rights reserved.
doi:10.1016/j.jsv.2008.09.040

conjunction with various integrations reduces the distributed-parameter problem to a discrete problem of finding the unknown coefficients of the series expansion.

The series discretization methods can be classified into two broad categories: variational approaches and the method of weighted residuals. The most common variational approach is the Rayleigh–Ritz method [1–7]. Depending on the type of formulation, the trial functions are chosen from either comparison or admissible functions. The method is imposed by determining the combination of the trial functions that will render Rayleigh's quotient stationary. Although the Rayleigh–Ritz method is a powerful approach, it is only applicable to linear self-adjoint systems [8]. Furthermore, the method does not provide direct solution for the problems with forcing functions, but rather necessitates the use of the modal expansion technique to obtain solutions. In addition, when the boundary conditions are complex, finding trial functions that are admissible functions poses considerable challenges.

A closely related technique is the assumed modes method [9–14]. In this method, a series form of eigenfunctions is assumed. However, instead of using a variational approach directly, Lagrange's equations are utilized to obtain the spatially discretized equations of motion. Indeed, since Lagrange's equations are derived using a variational approach (Hamilton's principle), the assumed modes method is also considered as a variational approach. Accordingly, the technique is only applicable to self-adjoint systems.

Unlike the Rayleigh–Ritz techniques, the method of weighted residuals can directly work with the partial differential equation [8]. An approximate solution is considered in the form of a finite series with trial functions from the space of admissible functions. To minimize the error, or the *residual*, arising from the truncation of the infinite series, the inner product of the residuals and weighting functions (also from the space of admissible functions) is required to vanish. The most common method of weighted residuals is Galerkin's method [15–20], in which the weighting functions coincide with the trial functions. The main advantages of the method of weighted residuals include its applicability to both self-adjoint and nonself-adjoint systems (including linear and nonlinear problems); and its capability to directly solve problems with forcing functions without resorting to the modal expansion technique.

The convergence and accuracy of the method of weighted residuals depend greatly on the choice trial functions. To make the trial and weighting functions admissible, common applications of the weighted residuals technique require each function to satisfy the geometric boundary conditions. In the previous works, researchers used power series [20,21]; trigonometric series [21]; and special polynomials such as Legendre [15] and Hermitian polynomials [19] as trial functions. Some researchers used the mode shapes from a simplified version of the original problem as trial functions [16–18]. In order to satisfy the geometric boundary conditions, supplementary polynomial terms are added to the basis functions. In doing so, however, a new formulation was required (i.e., new trial functions must be selected) for each problem with different boundary conditions.

Although generally considered an exact method rather than an approximate method, the dynamic stiffness matrix technique is worth mentioning here [22–27]. In this powerful technique, a function that satisfies the spatial differential equations is considered with undetermined coefficients. The geometric and natural boundary conditions are then described in separate matrix forms. Solution of the coefficient matrix from the geometric boundary conditions and substitution of this solution to the natural boundary condition matrix equation yield the dynamic stiffness matrix [28]. In general, this solution technique requires solving transcendental equations to find the eigenvalues rather than using the standard eigenvalue solvers. For beams with complex geometries and boundary conditions, determination of eigenvalues from the dynamic stiffness matrix necessitates the use of special algorithms, such as that of William–Wittrick [29]. The derivation of the dynamic stiffness matrix can be carried out numerically or analytically, latter of which requires lengthily symbolic manipulations. For each boundary condition and beam type (e.g., tapered or twisted beams), a different dynamic stiffness matrix is required. The dynamic stiffness matrix method has been used to solve various problems including coupled bending/torsional motions [30–32], spinning beam dynamics [33,34], and twisted beams [35].

Due to their recursive nature and fast convergence characteristics, Tchebychev orthogonal polynomials have been used in the literature for the solution of boundary-value problems [36–40,7,41]. Lovejoy and Kapania [40] and Singhvi and Kapania [7] used Tchebychev polynomials with Rayleigh–Ritz method. The geometric BCs were satisfied by using fictitious springs with sufficiently high stiffness. Singhvi and Kapania [7]

showed that orthogonal Tchebychev polynomials work more efficiently than simple polynomials. Lee and Schultz [39] applied Tchebychev collocation and pseudo-spectral weighted residual method to solve the vibration of Timoshenko beams and Mindlin plates. Ruta [36–38] also utilized Tchebychev polynomials to solve various beam problems. However, in Ruta's work the self-adjointness was not preserved after the discretization, resulting in complex natural frequencies. Additionally, since the boundary conditions were not fully satisfied, the higher modes could not be accurately determined. Gottlieb and Orszag [41] compared the convergence characteristics of various recursive polynomials, and concluded that the Tchebychev polynomials were superior especially in handling the boundaries.

In this paper, a new approach for solving linear and nonlinear beam problems in structural dynamics is presented. This *spectral-Tchebychev technique* uses Tchebychev polynomials as the basis for the spatial discretization. A weak convergence similar to that in Galerkin's method is considered. However, unlike the alternative approaches, the spectral-Tchebychev technique incorporates geometric and natural boundary conditions through projection matrices (basis recombination) as an integral part of the approach, rather than requiring the trial functions to be chosen from admissible functions. This allows formulating the solution with generic boundary conditions, and enables obtaining simple solutions that are applicable to a wide range of linear and nonlinear problems. Using the spectral-Tchebychev technique, the forced response can be obtained directly, without resorting to the modal expansion technique. Most importantly, the technique produces symmetric system matrices for the self-adjoint problems, i.e., the technique is equivalent to variational approaches for self-adjoint problems. This symmetry results from the fact that derivatives, integrals and inner products are computed *exactly* for any function that can be expressed by N-Tchebychev polynomials. Furthermore, the technique is applicable to nonself-adjoint problems.

The paper first describes the notation and briefly reviews the properties of Tchebychev polynomials and expansions. Next, the spectral-Tchebychev technique is explained. To simplify the explanation, the wave equation with generic boundary conditions and the nonuniform parameter distribution is solved using the spectral-Tchebychev technique. The derivation of the spectral-Tchebychev technique for the Euler–Bernoulli and Timoshenko beams with generic boundary conditions are then described. This is followed by an evaluation of the numerical accuracy and convergence of the spectral-Tchebychev technique by considering eigenvalue problems for both Euler–Bernoulli and Timoshenko beams with different boundary conditions. The spectral-Tchebychev technique is then applied to an Euler–Bernoulli beam with an elastic boundary and spatially varying forcing function; and to a tapered Timoshenko beam with different boundary conditions and taper ratios. Application of the technique to nonlinear problems is illustrated by two examples from the literature, including a large-deflection beam with base excitation, and an electrostatically excited micro-beam. In both cases, the results obtained using the spectral-Tchebychev technique are in excellent agreement with the experimental and modeling results given in the literature.

2. Summary of notation

In this section, the basic properties of Tchebychev polynomials and Tchebychev expansions that can be found in the literature (e.g., Refs. [41–43]) are briefly reviewed, and the notation that will be used throughout the paper is introduced.

2.1. Tchebychev polynomials and Tchebychev expansion

The Tchebychev polynomials are recursive orthogonal polynomials that can be described as

$$T_k(x) = \cos(k \cos^{-1}(x)) \quad \text{for } k = 0, 1, 2, \ldots, \tag{1}$$

where k is an integer [41]. Although defined for all x, Tchebychev polynomials are a stable representation only on the $(-1, 1)$ interval. In this interval, they form a complete set, which means that any square-integrable function $y(x)$ can be represented by a series expansion using the Tchebychev polynomials as the basis.

Since most functions of interest lie on the interval (ℓ_1, ℓ_2) instead of $(-1, 1)$, a mapping between $x \in (\ell_1, \ell_2)$ and $\xi \in (-1, 1)$ is defined as

$$x(\xi) = \xi \frac{\ell_2 - \ell_1}{2} + \frac{\ell_2 + \ell_1}{2} \quad \text{and} \quad \xi(x) = \frac{2}{\ell_2 - \ell_1} x - \frac{\ell_2 + \ell_1}{\ell_2 - \ell_1}. \tag{2}$$

When considering functions on the interval (ℓ_1, ℓ_2), the scaled Tchebychev polynomials $\mathscr{T}_k(x) = T_k(\xi(x))$ are used.

A function $y(x) \in (\ell_1, \ell_2)$ can be expressed using the Tchebychev series expansion as

$$y(x) = \sum_{k=0}^{\infty} a_k \mathscr{T}_k(x). \tag{3}$$

If a square-integrable function $y(x)$ is also infinitely differentiable on the interval (ℓ_1, ℓ_2), then the coefficients a_k in Tchebychev expansion decay exponentially with increasing k value. This exponential decay is a result of the fact that Tchebychev polynomials are eigenfunctions of the singular Sturm–Liouville problem [41]. Although the Legendre, Hermite, and Laguerre polynomials are also eigenfunctions of the Sturm–Liouville problem, Tchebychev polynomials are more effective in handling the boundaries [41]. Therefore, if the function $y(x)$ is well behaved on the interval (ℓ_1, ℓ_2) (i.e., it does not possess a narrow spike or a region of very large derivatives), a relatively small number of terms will be sufficient to accurately represent the function. Thus, for numerical solutions, the function $y(x)$ can be expressed as

$$y_N(x) = \sum_{k=0}^{N-1} a_k \mathscr{T}_k(x), \tag{4}$$

where N is the number of polynomials used for the truncated expansion. The exponential convergence behavior of the Tchebychev expansion allows accurate representation of functions and estimation of the error caused by the truncation. For brevity of notation, the subscript N in y_N will be omitted in the remainder of the paper.

It is important to note here that a continuous function that is expressible by N-Tchebychev polynomials can be described *exactly* by N coefficients of Tchebychev expansion. While this representation includes N discrete values, since it describes the sum of continuous Tchebychev polynomials, it must still be viewed as a continuous function.

2.2. Gauss–Lobatto sampling and Tchebychev expansion coefficients

For numerical calculations, a continuous function is represented by a vector of points sampled (spatially) at certain increments. Irrespective of the way the function is sampled, if the function is expressible by N-Tchebychev polynomials and spatially sampled at N points $\{x_k\}_{k=1}^{N}$, there exists a one-to-one mapping between the expansion coefficients a_k and the sampled points $y_k = y(x_k)$. This means that a function can be defined by either using coefficients a_k or giving its values $y_k = y(x_k)$ at the Gauss–Lobatto points. The relationship between the vector of sampled function $\mathbf{y} = \{y_k\}$ and the (truncated) Tchebychev expansion coefficient vector $\mathbf{a} = \{a_k\}$ can be written as

$$\mathbf{a} = \mathbf{\Gamma}_F \mathbf{y}, \tag{5}$$

where $\mathbf{\Gamma}_F$ is an $N \times N$ *forward transformation* matrix (see Appendix A). A *backward transformation* can also be written as

$$\mathbf{y} = \mathbf{\Gamma}_B \mathbf{a}, \tag{6}$$

where

$$\mathbf{\Gamma}_B \mathbf{\Gamma}_F = \mathbf{\Gamma}_F \mathbf{\Gamma}_B = \mathbb{I}, \tag{7}$$

and $\mathbb{I}$ is the identity matrix.

The relationship between the sampled points and the Tchebychev coefficients, i.e., $\mathbf{\Gamma}_B$ and $\mathbf{\Gamma}_F$ matrices, become simpler and easier to compute if the sampling is performed at the Gauss–Lobatto points

described as

$$p_k = \cos\left(\frac{(k-1)\pi}{N-1}\right), \quad k = 1, 2, \ldots, N \tag{8}$$

defined on the $(-1, 1)$ interval. The scaled Gauss–Lobatto points are defined on the interval (ℓ_1, ℓ_2) as

$$x_k = x(p_k), \tag{9}$$

where $x(\xi)$ is the mapping given in Eq. (2).

2.3. Differentiation, integration, and inner products

The truncated Tchebychev expansion of the spatial derivative y' of the function y can be written as

$$y'(x) = \sum_{k=0}^{N-1} b_k \mathscr{T}_k(x). \tag{10}$$

It can be shown that (see Appendix B) the coefficients a_k and b_k are related through a differentiation matrix $\mathbf{D}$ in the Tchebychev space as

$$\mathbf{b} = \mathbf{D}\mathbf{a}. \tag{11}$$

Similarly, the expansion coefficients $a_k^{(n)}$ of the nth spatial derivative of y can be given as

$$\mathbf{a}^{(n)} = \mathbf{D}^n \mathbf{a}. \tag{12}$$

Using the transformation matrices described above, relationship in the physical (sampled) space can be obtained as

$$\mathbf{y}^{(n)} = \mathbf{\Gamma}_B \mathbf{a}^{(n)} = \mathbf{\Gamma}_B \mathbf{D}^n \mathbf{\Gamma}_F \mathbf{y} = \mathbf{Q}_n \mathbf{y}, \tag{13}$$

where $\mathbf{y}^{(n)}$ is the sampled vector for the nth-derivative of $y(x)$, and $\mathbf{Q}_n$ is the nth derivative matrix. If $y(x)$ can be expressed *exactly* using N-Tchebychev polynomials, then $y^{(n)}(x)$ can be computed exactly from Eq. (13).

The definite integral of a function $y(x)$ can be described as

$$\int_{\ell_1}^{\ell_2} y(x)\,\mathrm{d}x = \mathbf{v}^{\mathrm{T}}\mathbf{a}, \tag{14}$$

where $\mathbf{v}$ is the definite integral vector and $\mathbf{a}$ is the coefficient vector given in Eq. (5) (see Appendix C). If $y(x)$ is expressed *exactly* using N-Tchebychev polynomials, the integral of $y(x)$ in the interval (ℓ_1, ℓ_2) can then be computed *exactly* from Eq. (14).

The inner product of two functions $y(x)$ and $f(x)$ that can be expressed by Tchebychev polynomials as

$$\int_{\ell_1}^{\ell_2} f(x)g(x)\,\mathrm{d}x = \mathbf{f}^{\mathrm{T}}\mathbf{V}\mathbf{g}, \tag{15}$$

where $\mathbf{V}$ is the inner-product matrix (see Appendix D). Again, if N-polynomial representation of the two functions is exact, this integral is computed exactly through Eq. (15).

The recursive relations used to compute the transformation ($\mathbf{\Gamma}_F$, $\mathbf{\Gamma}_B$), derivative ($\mathbf{D}$), definite integral ($\mathbf{v}$), and inner product ($\mathbf{V}$) matrices are provided in the Appendix section.

3. Method development—the wave equation

This section describes the spectral-Tchebychev technique for solving the wave equation. The steps described below for the derivation of the spectral-Tchebychev technique will be applied in a similar fashion to solve beam equations.

The wave equation that describes the longitudinal vibrations of a beam can be expressed as

$$\rho A \ddot{y}^* = (EAy^{*\prime})' + f^*(x^*, t^*) \quad \text{defined on } 0 < x^* < L, \tag{16}$$

where ρ is the density, A is the cross-sectional area, E is Young's modulus, L is the length of the beam, y is the axial deflection and f is the forcing function, prime ($'$) indicates the spatial derivative, and dot ($\cdot$) indicates the temporal derivative. Starred letters represent the dimensional parameters. When the parameters are uniformly distributed along the beam, the wave equation can be nondimensionalized as

$$\ddot{y} = \mu y'' + f \quad \text{defined on } 0<x<1, \tag{17}$$

subjected to the boundary conditions

$$(\beta_{10}y' + \beta_{00}y)|_{x=0} = \alpha_0(t), \quad (\beta_{1L}y' + \beta_{0L}y)|_{x=L} = \alpha_L(t), \tag{18}$$

where the nondimensional parameters are defined as

$$x = x^*/L, \quad y = y^*/L, \quad t = t^*\omega_0, \quad \mu = \frac{E}{\rho L^2\omega_0^2}, \quad f = \frac{f^*}{\rho AL\omega_0^2}. \tag{19}$$

Here ω_0 is a frequency (commonly chosen as the first natural frequency) used for nondimensionalizing the time. β's are the constant coefficients of the spatial part of the boundary conditions and α's describe the temporal part of the boundary conditions. By specifying the coefficients β and $\alpha(t)$, Eq. (18) can be used to prescribe various linear boundary conditions. The system described in Eqs. (17) and (18) is a self-adjoint system.

It should be noted here that the spectral-Tchebychev technique presented here is applicable to other types of linear boundary conditions (e.g., mixed boundary conditions) that are not covered by the form given in Eq. (18). The most generic linear boundary conditions can be written as

$$\sum_{k=0}^{1}\sum_{p=0,L} \Upsilon_{kps}y^{(k)} = \alpha_s(t), \tag{20}$$

where Υ_{kps}'s are the constant coefficients of the spatial part of the boundary conditions and α_s is the temporal part of the boundary conditions. Condition p denotes the particular boundary ($p = 0, L$), k is the order of derivative, and s is the number of the boundary condition (i.e., $s = 1, 2$ since the wave equation is second-order). Although with Eq. (20) any set of linear boundary conditions can be considered in the spectral-Tchebychev technique, Eq. (18) is used in the rest of the derivation to simplify the discussion and to retain the self-adjointness of the problem.

The spatially discretized version of our problem arises from assuming that the function is expressible in terms of N scaled Tchebychev polynomials. As discussed in Section 2.2, any such function can be defined by giving its values at the Gauss–Lobatto points. Therefore, the spatially sampled version of Eq. (17) is written as

$$\ddot{\mathbf{y}} = \mu\mathbf{y}'' + \mathbf{f}, \tag{21}$$

where the vectors (lower-case, bold) are obtained by spatially sampling the continuous functions at the Gauss–Lobatto points. This equation is further manipulated by describing the spatial derivatives using the properties of Tchebychev expansion as

$$\ddot{\mathbf{y}} = \mu\mathbf{Q}_2\mathbf{y} + \mathbf{f}, \tag{22}$$

where $\mathbf{Q}_2$ is the second-derivative matrix (see Eq. (13)). Similarly, the boundary conditions (from Eq. (18)) can be written as

$$\boldsymbol{\beta}\mathbf{y} = \boldsymbol{\alpha}, \tag{23}$$

where

$$\boldsymbol{\beta} = \begin{bmatrix} \boldsymbol{\beta}_{10}\mathbf{e}_1^{\mathrm{T}}\mathbf{Q}_1 + \boldsymbol{\beta}_{00}\mathbf{e}_1^{\mathrm{T}} \\ \boldsymbol{\beta}_{1L}\mathbf{e}_N^{\mathrm{T}}\mathbf{Q}_1 + \boldsymbol{\beta}_{0L}\mathbf{e}_N^{\mathrm{T}} \end{bmatrix} \quad \text{and} \quad \boldsymbol{\alpha} = \begin{Bmatrix} \boldsymbol{\alpha}_0(t) \\ \boldsymbol{\alpha}_L(t) \end{Bmatrix}. \tag{24}$$

Here, $\mathbf{Q}_1$ is the first-derivative matrix (see Eq. (13)), and $\mathbf{e}_j$ is an N-vector whose jth element is unity and all other elements are zeros.

An effective way of imposing the boundary condition is to express $\mathbf{y}$ using projection matrices as

$$\mathbf{y} = \mathbf{P}\mathbf{z} + \mathbf{R}\boldsymbol{\alpha}, \tag{25}$$

where $\mathbf{P}$ and $\mathbf{R}$ are $N \times (N - M)$ and $N \times M$ projection matrices, respectively, and $\mathbf{z}$ is an $(N - M)$-vector, where M is the number of boundary conditions. This procedure is also referred to as *basis recombination*. Eq. (25) allows solving for $\mathbf{z}$, which satisfies only the homogeneous boundary conditions, while ensuring $\mathbf{y}$ satisfies all the boundary conditions. Numerically, $\mathbf{P}$ and $\mathbf{R}$ matrices are determined using the singular-value of $\boldsymbol{\beta}$ (see Appendix F for details). Substituting Eq. (25) into Eq. (22) gives

$$\mathbf{P}\ddot{\mathbf{z}} + \mathbf{R}\ddot{\boldsymbol{\alpha}} = \mu\mathbf{Q}_2(\mathbf{P}\mathbf{z} + \mathbf{R}\boldsymbol{\alpha}) + \mathbf{f}. \tag{26}$$

It should be recognized that Eq. (26) is an approximation. The error, or residual, arising from this approximation can be expressed as

$$\boldsymbol{\phi} = \mathbf{P}\ddot{\mathbf{z}} + \mathbf{R}\ddot{\boldsymbol{\alpha}} - \mu\mathbf{Q}_2(\mathbf{P}\mathbf{z} + \mathbf{R}\boldsymbol{\alpha}) - \mathbf{f}. \tag{27}$$

In order to minimize the error, the weighted residuals method will be used, and the inner product of the weighted residuals will be required to vanish, viz.,

$$\int_{\ell_1}^{\ell_2} \theta(x)\phi(x)\,\mathrm{d}x = 0, \tag{28}$$

where $\theta(x)$ are the weighting functions. If $\theta(x)$ are also chosen to coincide with the trial functions (i.e., expressible by an N-polynomial Tchebychev expansion), this particular method of weighted residuals is referred to as *Galerkin's method* [8]. Using the inner-product expression from Section 2.3, Eq. (28) is rewritten as the

$$\int_{\ell_1}^{\ell_2} \theta(x)\phi(x)\,\mathrm{d}x = \boldsymbol{\theta}^{\mathrm{T}}\mathbf{V}\boldsymbol{\phi}. \tag{29}$$

Here, it will be required that the weighting functions satisfy the homogeneous boundary conditions. Mathematically, this conditions can be expressed as $\boldsymbol{\theta} = \mathbf{P}\bar{\boldsymbol{\theta}}$ considering Eq. (25).

Substituting Eq. (27) into Eq. (29), after rearranging

$$\bar{\boldsymbol{\theta}}^{\mathrm{T}}\{\mathbf{P}^{\mathrm{T}}\mathbf{V}[(\mathbf{P}\ddot{\mathbf{z}} - \mu\mathbf{Q}_2\mathbf{P}\mathbf{z}) - (\mathbf{f} - \mathbf{R}\ddot{\boldsymbol{\alpha}} + \mu\mathbf{Q}_2\mathbf{R}\boldsymbol{\alpha})]\} = 0. \tag{30}$$

Since this equation must be satisfied for arbitrary $\bar{\boldsymbol{\theta}}$, the quantity inside the square brackets must be zero, i.e.,

$$\mathbf{P}^{\mathrm{T}}\mathbf{V}\mathbf{P}\ddot{\mathbf{z}} - \mu\mathbf{P}^{\mathrm{T}}\mathbf{V}\mathbf{Q}_2\mathbf{P}\mathbf{z} = \mathbf{P}^{\mathrm{T}}\mathbf{V}\mathbf{f} - \mathbf{P}^{\mathrm{T}}\mathbf{V}\mathbf{R}\ddot{\boldsymbol{\alpha}} + \mu\mathbf{P}^{\mathrm{T}}\mathbf{V}\mathbf{Q}_2\mathbf{R}\boldsymbol{\alpha}. \tag{31}$$

This equation can be expressed in the form

$$\mathbf{M}\ddot{\mathbf{z}} + \mathbf{K}\mathbf{z} = \hat{\mathbf{f}}, \tag{32}$$

where

$$\mathbf{M} = \mathbf{P}^{\mathrm{T}}\mathbf{V}\mathbf{P}, \quad \mathbf{K} = -\mu\mathbf{P}^{\mathrm{T}}\mathbf{V}\mathbf{Q}_2\mathbf{P}$$

and

$$\hat{\mathbf{f}} = \mathbf{P}^{\mathrm{T}}\mathbf{V}\mathbf{f} - \mathbf{P}^{\mathrm{T}}\mathbf{V}\mathbf{R}\ddot{\boldsymbol{\alpha}} + \mu\mathbf{P}^{\mathrm{T}}\mathbf{V}\mathbf{Q}_2\mathbf{R}\boldsymbol{\alpha}. \tag{33}$$

The $\mathbf{M}$ and $\mathbf{K}$ matrices in these expressions are guaranteed to be symmetric for self-adjoint problems. A detailed explanation on how self-adjointness is preserved is given in Appendix E.

To obtain the numerical solution, Eq. (32) can be represented in the state-space form, and an (temporal) integration algorithm can be used. To represent the system in the state-space form, the transformation $\mathbf{z} = \mathbf{M}^{-1/2}\mathbf{p}$ will be defined, and Eq. (32) will be rewritten as

$$\mathbf{M}\mathbf{M}^{-1/2}\ddot{\mathbf{p}} + \mathbf{K}\mathbf{M}^{-1/2}\mathbf{p} = \hat{\mathbf{f}}. \tag{34}$$

Left-multiplying both sides by $\mathbf{M}^{-1/2}$ results in

$$\mathbb{I}\ddot{\mathbf{p}} + \mathbf{M}^{-1/2}\mathbf{K}\mathbf{M}^{-1/2}\mathbf{p} = \mathbf{M}^{-1/2}\hat{\mathbf{f}}, \tag{35}$$

where $\mathbf{M}^{-1/2}\mathbf{K}\mathbf{M}^{-1/2}$ is guaranteed to be symmetric for any nonsingular symmetric matrix $\mathbf{K}$. When calculating $\mathbf{M}^{-1/2}$, it is advisable to write

$$\mathbf{M} = \mathbb{M}\Lambda\mathbb{M}^{\mathrm{T}} \quad \text{and} \quad \mathbf{M}^{-1/2} = \mathbb{M}\Lambda^{-1/2}\mathbb{M}^{\mathrm{T}}, \tag{36}$$

where $\mathbb{M}$ is the eigenvector matrix of $\mathbf{M}$ and Λ is a diagonal matrix with the eigenvalues of $\mathbf{M}$ in its diagonal. The state-space form can now be written as

$$\dot{\mathbf{q}} = \mathbb{A}\mathbf{q} + \mathbb{B}\hat{\mathbf{f}} \quad \text{and} \quad \mathbf{p} = \mathbb{G}\mathbf{q}, \tag{37}$$

where

$$\mathbb{A} = \begin{bmatrix} 0 & \mathbb{I} \\ -\mathbf{M}^{-1/2}\mathbf{K}\mathbf{M}^{-1/2} & 0 \end{bmatrix}, \quad \mathbb{B} = \begin{bmatrix} 0 \\ \mathbf{M}^{-1/2} \end{bmatrix} \quad \text{and} \quad \mathbb{G} = [\mathbb{I}\ 0]. \tag{38}$$

To obtain the solution of the boundary-value problem given in Eq. (17), $\mathbf{q}$ is solved and $\mathbf{p}$ is determined from Eq. (37). Substituting $\mathbf{p}$ in $\mathbf{z} = \mathbf{M}^{-1/2}\mathbf{p}$, and subsequently using Eq. (25), $\mathbf{y}$ is obtained. If continuous functions are sought, the associated Tchebychev expansion coefficients a_k can be found from Eq. (5), and the solution can be written as a continuous function through the Tchebychev expansion.

The spectral-Tchebychev technique can be extended to the problems with *spatially varying parameters*. To handle this situation without compromising the symmetry of system matrices, the application of the spectral-Tchebychev technique is modified. To illustrate this modification, the cross-sectional area in Eq. (16) is considered to vary with x^*. The new nondimensional equation of motion is written as

$$A\ddot{y} = \mu_p[Ay']' + f \quad \text{defined on } 0 < x < 1, \tag{39}$$

where

$$x = x^*/L, \quad y = y^*/L, \quad t = t^*\omega_0, \quad A = A(x^*)/L^2, \tag{40}$$

$$\mu_p = \frac{E}{\rho L^2\omega_0^2}, \quad f = \frac{f^*}{\rho L^3\omega_0^2}. \tag{41}$$

After applying the chain rule, Eq. (39) becomes

$$A\ddot{y} = \mu_p[A'y' + Ay''] + f \quad \text{defined on } 0 < x < 1. \tag{42}$$

To retain the symmetry while handling this problem, new inner products are defined as

$$\int_{\ell_1}^{\ell_2} \theta(x)\phi(x)A(x)\,\mathrm{d}x = \boldsymbol{\theta}^{\mathrm{T}}\mathbf{V}_A\boldsymbol{\phi}, \tag{43}$$

$$\int_{\ell_1}^{\ell_2} \theta(x)\phi(x)A'(x)\,\mathrm{d}x = \boldsymbol{\theta}^{\mathrm{T}}\mathbf{V}_{A'}\boldsymbol{\phi}. \tag{44}$$

The derivative of the area is computed in the spatially discretized domain by following Eq. (12) as $\mathbf{A}' = \mathbf{Q}_1\mathbf{A}$. These inner-product matrices are calculated exactly for functions that are described by N-Tchebychev polynomials. Using these inner products, Eq. (42) becomes

$$\mathbf{P}^{\mathrm{T}}\mathbf{V}_A\mathbf{P}\ddot{\mathbf{z}} - \mu_p\mathbf{P}^{\mathrm{T}}(\mathbf{V}_{A'}\mathbf{Q}_1 + \mathbf{V}_A\mathbf{Q}_2)\mathbf{P}\mathbf{z} = \mathbf{P}^{\mathrm{T}}\mathbf{V}\mathbf{f} - \mathbf{P}^{\mathrm{T}}\mathbf{V}_A\mathbf{R}\ddot{\boldsymbol{\alpha}} + \mu_p\mathbf{P}^{\mathrm{T}}(\mathbf{V}_{A'}\mathbf{Q}_1 + \mathbf{V}_A\mathbf{Q}_2)\mathbf{R}\boldsymbol{\alpha}, \tag{45}$$

which can be represented in the same form as Eq. (32) by defining

$$\mathbf{M} = \mathbf{P}^{\mathrm{T}}\mathbf{V}_A\mathbf{P}, \quad \mathbf{K} = -\mu_p\mathbf{P}^{\mathrm{T}}(\mathbf{V}_{A'}\mathbf{Q}_1 + \mathbf{V}_A\mathbf{Q}_2)\mathbf{P}$$

and

$$\hat{\mathbf{f}} = \mathbf{P}^{\mathrm{T}}\mathbf{V}\mathbf{f} - \mathbf{P}^{\mathrm{T}}\mathbf{V}_A\mathbf{R}\ddot{\boldsymbol{\alpha}} + \mu_p\mathbf{P}^{\mathrm{T}}(\mathbf{V}_{A'}\mathbf{Q}_1 + \mathbf{V}_A\mathbf{Q}_2)\mathbf{R}\boldsymbol{\alpha}. \tag{46}$$

The $\mathbf{M}$ and $\mathbf{K}$ matrices given above are guaranteed to be symmetric for self-adjoint systems.

In summary, the dependent variable $y(x,t)$ of the boundary-value problem was described by a series expansion using N-Tchebychev polynomials as the spatial basis functions. Instead of imposing the boundary conditions on individual trial functions, a projection is defined to incorporate the boundary conditions directly into the derivation. The Galerkin's method was then used to minimize the residual arising from the truncation of the infinite series. As a result, a simple matrix equation that describes the spatially discretized version of the system was derived. The system equations were symmetric for the self-adjoint wave equation, indicating that the spectral-Tchebychev method is equivalent to variational approaches for the case of self-adjoint problems. This property is very critical for the numerical stability and efficiency of the technique, and follows from the exact evaluation of differentiation and inner-product operations using the Tchebychev matrix operators, as well as the use of Galerkin's method.

4. Spectral-Tchebychev technique for Euler–Bernoulli and Timoshenko beams

4.1. The Euler–Bernoulli model

The equation of motion for a linear Euler–Bernoulli beam can be given as

$$\rho A\ddot{y}^* + (EIy''^*)'' = f^*(x^*,t^*), \quad 0<x^*<L. \tag{47}$$

For a beam with uniform parameters, the nondimensional form of this equation can be given as

$$m\ddot{y} + y'''' = f(x,t), \quad 0<x<1 \tag{48}$$

subjected to the (generic) boundary conditions

$$(\beta_{ij3}y'''' + \beta_{ij2}y'' + \beta_{ij1}y' + \beta_{ij0}y)|_{x=x_i} = \alpha_{ij}(t), \quad i=0,L \text{ and } j=1,2, \tag{49}$$

where

$$x = x^*/L, \quad y = y^*/L, \quad t = t^*\omega_0, \quad m = \frac{\rho A\omega_0^2 L^4}{EI}, \quad f = \frac{f^*L^3}{EI}, \tag{50}$$

and I is the area moment of inertia.

Here $y(x,t)$ is the transverse deflection of the beam and $f(x,t)$ is the forcing function. The β_{ijk} are the coefficients of the boundary conditions at the two ends ($i=0,L$) of the beam, each end with two boundary conditions ($j=1,2$).

The sampled version of Eq. (48) can be expressed as

$$m\ddot{\mathbf{y}} + \mathbf{Q}_4\mathbf{y} = \mathbf{f}, \tag{51}$$

where $\mathbf{Q}_4$ is the fourth-derivative matrix. The boundary conditions can be written as

$$\mathbf{e}_1^{\mathrm{T}}\sum_{k=0}^{3}\beta_{0jk}\mathbf{Q}_k\mathbf{y} = \alpha_{0j}, \quad \mathbf{e}_N^{\mathrm{T}}\sum_{k=0}^{3}\beta_{Ljk}\mathbf{Q}_k\mathbf{y} = \alpha_{Lj}, \quad j=1,2, \tag{52}$$

where $\mathbf{Q}_0 = \mathbb{I}$. Imposing the boundary conditions through the projection matrices as

$$\mathbf{y} = \mathbf{P}\mathbf{z} + \mathbf{R}\boldsymbol{\alpha}, \tag{53}$$

and substituting into Eq. (51)

$$m(\mathbf{P}\ddot{\mathbf{z}} + \mathbf{R}\ddot{\boldsymbol{\alpha}}) + \mathbf{Q}_4(\mathbf{P}\mathbf{z} + \mathbf{R}\boldsymbol{\alpha}) = \mathbf{f}. \tag{54}$$

Applying Galerkin's method as in Eqs. (28)–(31), the spatially discretized equations of motion becomes

$$m\mathbf{P}^{\mathrm{T}}\mathbf{V}\mathbf{P}\ddot{\mathbf{z}} + \mathbf{P}^{\mathrm{T}}\mathbf{V}\mathbf{Q}_4\mathbf{P}\mathbf{z} = \mathbf{P}^{\mathrm{T}}\mathbf{V}\mathbf{f} - m\mathbf{P}^{\mathrm{T}}\mathbf{V}\mathbf{R}\ddot{\boldsymbol{\alpha}} - \mathbf{P}^{\mathrm{T}}\mathbf{V}\mathbf{Q}_4\mathbf{R}\boldsymbol{\alpha}, \tag{55}$$

which can be written in the form

$$\mathbf{M}\ddot{\mathbf{z}} + \mathbf{K}\mathbf{z} = \hat{\mathbf{f}}. \tag{56}$$

This equation is ready for time integration through the state-space method.

For some combinations of coefficients β_{ijk}, the boundary-value problem described in Eqs. (48)–(49) is a self-adjoint problem. In those cases, the matrices $\mathbf{M}$ and $\mathbf{K}$ obtained through the spectral-Tchebychev technique are symmetric. As mentioned earlier, the symmetry is critical for numerical robustness of the solution technique.

4.2. The Timoshenko beam

As the length-to-thickness ratio reduces, the shear deformation effects that are neglected in the Euler–Bernoulli formulation become increasingly important. In those cases, the Timoshenko-beam equations, which contain the shear deformation and rotary inertia effects, are used. The general form of Timoshenko beam equations are

$$[k_s GA(y^{*\prime} - \psi^*)]' - \rho A\ddot{y}^* = -f^*(x^*, t^*), \quad 0 < x^* < L, \tag{57}$$

$$(EI\psi^{*\prime})' + k_s GA(y^{*\prime} - \psi^*) - \rho I\ddot{\psi}^* = -\Psi^*(x^*, t^*), \quad 0 < x^* < L. \tag{58}$$

For a uniform cross-section beam, the nondimensional form of the Timoshenko-beam equations can be written as

$$y'' - \psi' - \chi\ddot{y} = f(x, t), \quad 0 < x < 1, \tag{59}$$

$$\sigma\psi'' + y' - \psi - \tau\ddot{\psi} = \Psi(x, t), \quad 0 < x < 1, \tag{60}$$

where

$$x = x^*/L, \quad y = y^*/L, \quad t = t^*\omega_0, \quad \psi^* = \psi, \tag{61}$$

$$\chi = \frac{\rho L^2\omega_0^2}{k_s G}, \quad \tau = \frac{\rho I\omega_0^2}{k_s GA}, \quad f = -\frac{f^* L}{k_s GA}, \quad \sigma = \frac{EI}{k_s GAL^2}, \quad \Psi = -\frac{\Psi^*}{k_s GA}. \tag{62}$$

Here $y(x, t)$ is the nondimensional flexural displacement, $\psi(x, y)$ is the nondimensional slope, $f(x, t)$ is the applied nondimensional force, and $\Psi(x, t)$ is the applied moment, k_s is the shear coefficient, and G is the shear modulus.

The generic (linear) boundary conditions for this case can be written as

$$\sum_{k=0}^{1} \beta_{ijk}^{y} y^{(k)} + \sum_{k=0}^{1} \beta_{ijk}^{\psi} \psi^{(k)} = \alpha_{ij}(t), \tag{63}$$

where the β's are the coefficients of the boundary conditions at the two ends ($i = 0, L$) of the beam, each end with two boundary conditions ($j = 1, 2$). For example, the boundary conditions for a cantilever beam can be given by specifying

$$\beta_{010}^{y} = L, \quad \beta_{020}^{\psi} = 1, \quad \alpha_{01} = \alpha_{02} = 0,$$

$$\beta_{L11}^{\psi} = \frac{EI}{L}, \quad \beta_{L20}^{\psi} = -k_s GA, \quad \beta_{L21}^{y} = k_s GA, \quad \alpha_{L1} = \alpha_{L2} = 0 \tag{64}$$

and all other β's are zeros.

Using Tchebychev expansion, the (Gauss–Lobatto) sampled version of the boundary-value problem can be given as

$$\mathbf{Q}_2\mathbf{y} - \mathbf{Q}_1\boldsymbol{\psi} - \chi\ddot{\mathbf{y}} = \mathbf{f}, \tag{65}$$

$$\sigma\mathbf{Q}_2\boldsymbol{\psi} + \mathbf{Q}_1\mathbf{y} - \boldsymbol{\psi} - \tau\ddot{\boldsymbol{\psi}} = \boldsymbol{\Psi}, \tag{66}$$

subjected to boundary conditions

$$\mathbf{e}_1^{\mathrm{T}}\left(\sum_{k=0}^{1}[\beta_{0jk}^{y}\mathbf{Q}_k\mathbf{y}+\beta_{0jk}^{\psi}\mathbf{Q}_k\boldsymbol{\psi}]\right)=\alpha_{0j},\quad j=1,2, \tag{67}$$

$$\mathbf{e}_N^{\mathrm{T}}\left(\sum_{k=0}^{1}[\beta_{Ljk}^{y}\mathbf{Q}_k\mathbf{y}+\beta_{Ljk}^{\psi}\mathbf{Q}_k\boldsymbol{\psi}]\right)=\alpha_{Lj},\quad j=1,2. \tag{68}$$

Here, it was assumed that the same number of polynomials (N) was used to express both y and ψ.

The residuals associated with Eqs. (65) and (66) can be written as

$$\boldsymbol{\phi}_y=\mathbf{Q}_2\mathbf{y}-\mathbf{Q}_1\boldsymbol{\psi}-\chi\ddot{\mathbf{y}}-\mathbf{f}, \tag{69}$$

$$\boldsymbol{\phi}_\psi=\sigma\mathbf{Q}_2\boldsymbol{\psi}+\mathbf{Q}_1\mathbf{y}-\boldsymbol{\psi}-\tau\ddot{\boldsymbol{\psi}}-\boldsymbol{\psi}. \tag{70}$$

In order to minimize the error, the weighted residuals will be required to vanish as

$$\int_0^L\theta_y(x)\phi_y(x)\,\mathrm{d}x=0,\quad \int_0^L\theta_\psi(x)\phi_\psi(x)\,\mathrm{d}x=0, \tag{71}$$

where $\theta_y(x)$ and $\theta_\psi(x)$ are the weighting functions. Following Eq. (29), these inner products can be represented as

$$\int_0^L\theta_y(x)\phi_y(x)\,\mathrm{d}x=\boldsymbol{\theta}_y^{\mathrm{T}}\mathbf{V}\boldsymbol{\phi}_y,\quad \int_0^L\theta_\psi(x)\phi_\psi(x)\,\mathrm{d}x=\boldsymbol{\theta}_\psi^{\mathrm{T}}\mathbf{V}\boldsymbol{\phi}_\psi. \tag{72}$$

Substituting $\boldsymbol{\phi}_y$ and $\boldsymbol{\phi}_\psi$

$$\boldsymbol{\theta}_y^{\mathrm{T}}[\mathbf{V}(\mathbf{Q}_2\mathbf{y}-\mathbf{Q}_1\boldsymbol{\psi}-\chi\ddot{\mathbf{y}}-\mathbf{f})]=0, \tag{73}$$

$$\boldsymbol{\theta}_\psi^{\mathrm{T}}[\mathbf{V}(\sigma\mathbf{Q}_2\boldsymbol{\psi}+\mathbf{Q}_1\mathbf{y}-\boldsymbol{\psi}-\tau\ddot{\boldsymbol{\psi}}-\boldsymbol{\Psi})]=0. \tag{74}$$

Defining,

$$\mathbf{q}=\begin{bmatrix}\mathbf{y}\\ \boldsymbol{\psi}\end{bmatrix},\quad \boldsymbol{\theta}=\begin{bmatrix}\boldsymbol{\theta}_y\\ \boldsymbol{\theta}_\psi\end{bmatrix},\quad \mathbf{V}_s=\begin{bmatrix}\mathbf{V} & 0\\ 0 & \mathbf{V}\end{bmatrix},\quad \tilde{\mathbf{f}}=\begin{bmatrix}\mathbf{f}\\ \boldsymbol{\Psi}\end{bmatrix}, \tag{75}$$

the boundary-value problem can be written as

$$\boldsymbol{\theta}^{\mathrm{T}}\mathbf{V}_s(\mathbf{M}_s\ddot{\mathbf{q}}+\mathbf{K}_s\mathbf{q}-\mathbf{B}_s\tilde{\mathbf{f}})=0, \tag{76}$$

where

$$\mathbf{M}_s=\begin{bmatrix}-\chi\mathbb{I} & 0\\ 0 & -\tau\mathbb{I}\end{bmatrix},\quad \mathbf{K}_s=\begin{bmatrix}\mathbf{Q}_2 & -\mathbf{Q}_1\\ \mathbf{Q}_1 & \sigma\mathbf{Q}_2-\mathbb{I}\end{bmatrix},\quad \mathbf{B}_s=\begin{bmatrix}\mathbb{I} & 0\\ 0 & \mathbb{I}\end{bmatrix}. \tag{77}$$

The term $\mathbb{I}$ represents the identity matrix. Similarly, the boundary conditions can be written as

$$\begin{bmatrix}\mathbf{e}_1^{\mathrm{T}}\sum_{k=0}^{1}\beta_{01k}^{y}\mathbf{Q}_k & \mathbf{e}_1^{\mathrm{T}}\sum_{k=0}^{1}\beta_{01k}^{\psi}\mathbf{Q}_k\\ \mathbf{e}_1^{\mathrm{T}}\sum_{k=0}^{1}\beta_{02k}^{y}\mathbf{Q}_k & \mathbf{e}_1^{\mathrm{T}}\sum_{k=0}^{1}\beta_{02k}^{\psi}\mathbf{Q}_k\\ \mathbf{e}_N^{\mathrm{T}}\sum_{k=0}^{1}\beta_{L1k}^{y}\mathbf{Q}_k & \mathbf{e}_N^{\mathrm{T}}\sum_{k=0}^{1}\beta_{L1k}^{\psi}\mathbf{Q}_k\\ \mathbf{e}_N^{\mathrm{T}}\sum_{k=0}^{1}\beta_{L2k}^{y}\mathbf{Q}_k & \mathbf{e}_N^{\mathrm{T}}\sum_{k=0}^{1}\beta_{L2k}^{\psi}\mathbf{Q}_k\end{bmatrix}\mathbf{q}=\begin{bmatrix}\alpha_{01}\\ \alpha_{02}\\ \alpha_{L1}\\ \alpha_{L1}\end{bmatrix}=\boldsymbol{\alpha}. \tag{78}$$

Using the projection matrices as in Eq. (25) and imposing the condition that the weighting functions must satisfy the homogeneous boundary conditions as $\boldsymbol{\phi}=\mathbf{P}\bar{\boldsymbol{\phi}}$, Eq. (76) becomes

$$\bar{\boldsymbol{\theta}}^{\mathrm{T}}\mathbf{P}^{\mathrm{T}}\mathbf{V}_s(\mathbf{M}_s(\mathbf{P}\ddot{\mathbf{z}}+\mathbf{R}\ddot{\boldsymbol{\alpha}})+\mathbf{K}_s(\mathbf{P}\mathbf{z}+\mathbf{R}\boldsymbol{\alpha})-\mathbf{B}_s\tilde{\mathbf{f}})=0, \tag{79}$$

which entails

$$\mathbf{P}^{\mathrm{T}}\mathbf{V}_s\mathbf{M}_s\mathbf{P}\ddot{\mathbf{z}} + \mathbf{P}^{\mathrm{T}}\mathbf{V}_s\mathbf{K}_s\mathbf{P}\mathbf{z} = \mathbf{P}^{\mathrm{T}}\mathbf{V}_s\mathbf{B}_s\tilde{\mathbf{f}} - \mathbf{P}^{\mathrm{T}}\mathbf{V}_s\mathbf{M}_s\mathbf{R}\ddot{\boldsymbol{\alpha}} - \mathbf{P}^{\mathrm{T}}\mathbf{V}_s\mathbf{K}_s\mathbf{R}\boldsymbol{\alpha}. \tag{80}$$

This equation is in the general form of

$$\mathbf{M}\ddot{\mathbf{z}} + \mathbf{K}\mathbf{z} = \hat{\mathbf{f}}, \tag{81}$$

which can be numerically integrated using the state-space approach. For some boundary conditions, the boundary-value problem becomes a self-adjoint problem. For those problems, the system matrices **M** and **K** obtained above through the spectral-Tchebychev technique will be symmetric.

5. Method evaluation

To evaluate the accuracy and convergence of the spectral-Tchebychev solution, natural frequencies of Euler–Bernoulli and Timoshenko beams were calculated for four different boundary conditions using increasing number of polynomials. The calculated natural frequencies were compared to those computed from Newton's shooting method (with 10^{-11} resolution) [44].

Figs. 1(a)–(d) provide the error between the spectral-Tchebychev and Newton's shooting methods for the first five natural frequencies of an Euler–Bernoulli beam with pinned–pinned, fixed–fixed, fixed–pinned, and fixed–free boundary conditions, respectively. The parameters of the rectangular beam used for the computations include a length of $L = 0.5\,\mathrm{m}$, a width of $w = 0.05\,\mathrm{m}$, a thickness of $h = 0.01\,\mathrm{m}$, a density of

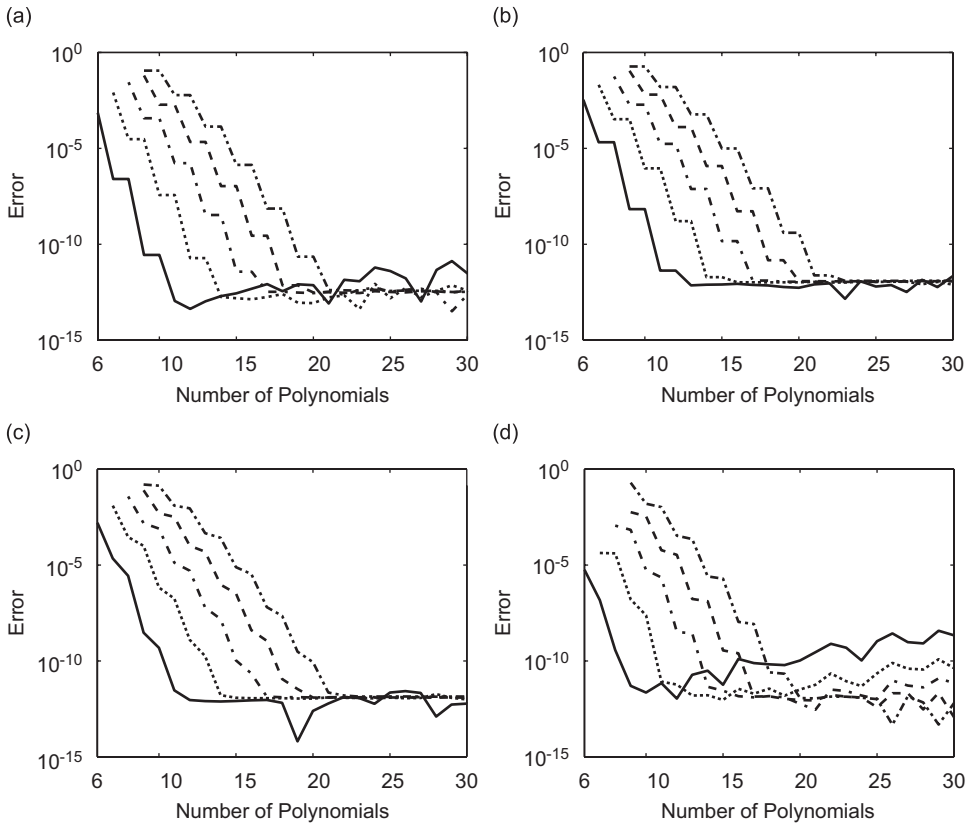

Fig. 1. The error between the spectral-Tchebychev and Newton's shooting methods for the first five natural frequencies of Euler–Bernoulli beams with (a) pinned–pinned, (b) fixed–fixed, (c) fixed–pinned, and (d) fixed–free boundary conditions (ω_1 —, ω_2 ⋯, ω_3 -·-, ω_4 - - -, ω_5 -···-).

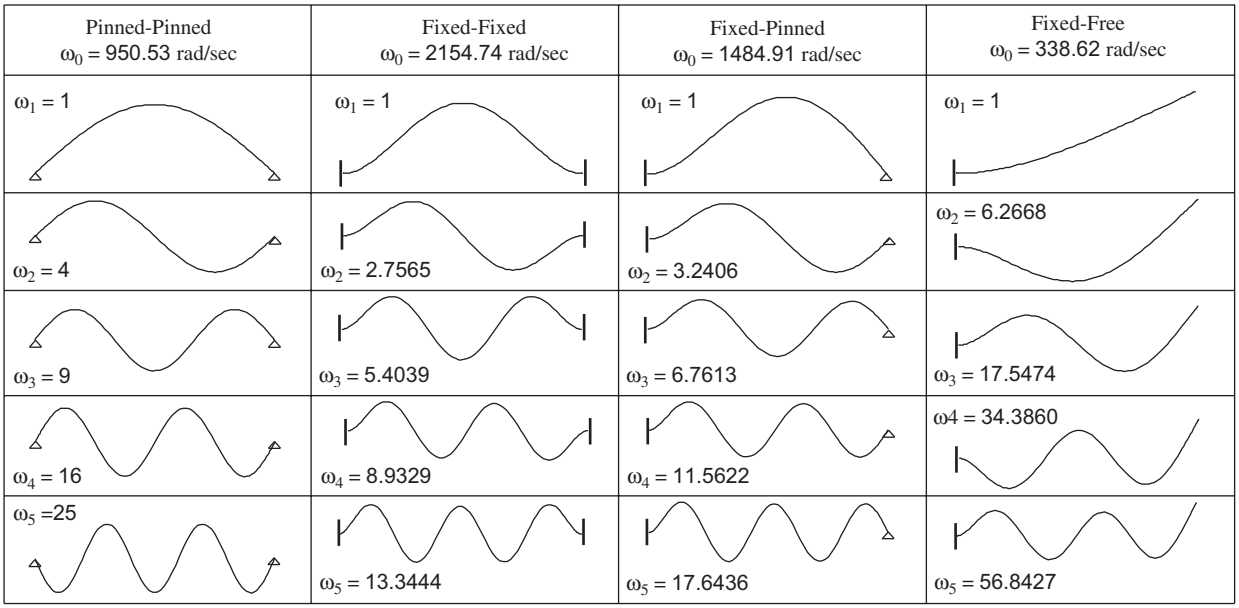

Fig. 2. First five mode shapes and normalized natural frequencies of Euler–Bernoulli beams with various boundary conditions. The natural frequencies are calculated using spectral-Tchebychev solution and normalized with respect to the first natural frequency ω_0 obtained from Newton's shooting method.

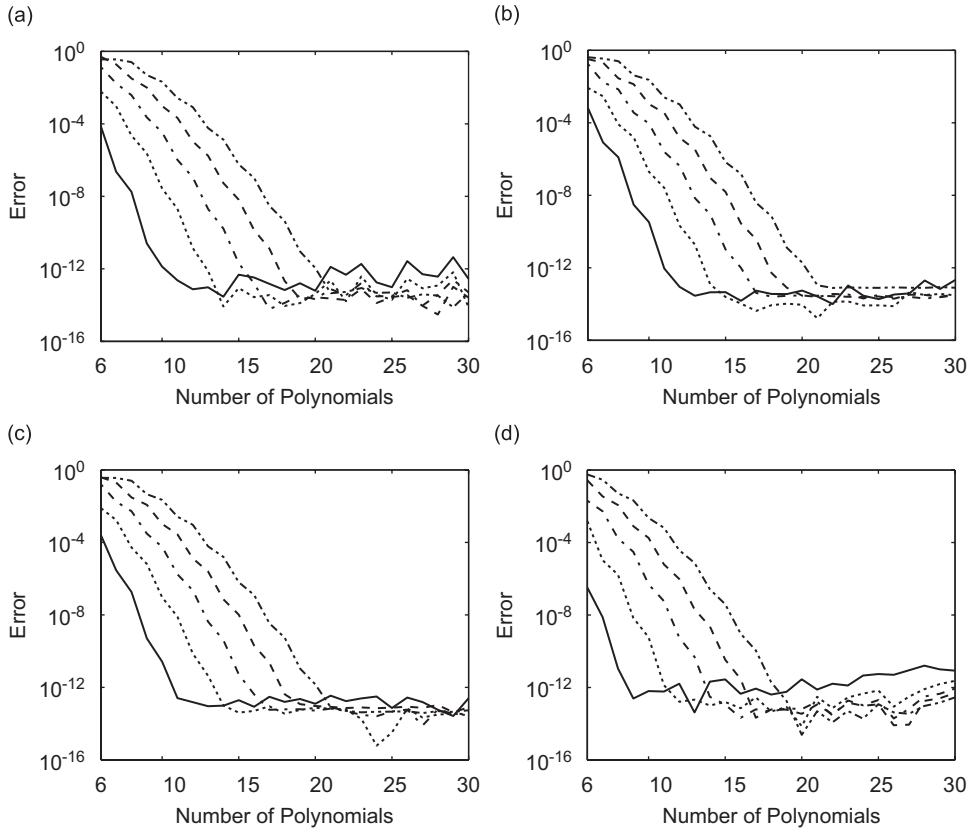

Fig. 3. The convergence of the first five natural frequencies of the Timoshenko beam with different boundary conditions. Boundary conditions in each case are (a) pinned–pinned, (b) fixed–fixed, (c) fixed–pinned, (d) fixed–free (ω_1 —, ω_2 ···, ω_3 -·-, ω_4 - - -, ω_5 -···-).

$\rho = 2300\,\mathrm{kg/m^3}$, and Young's modulus of $E = 160\,\mathrm{GPa}$. The error err_N is defined as

$$\mathrm{err}_N = \frac{|\omega_{N,k} - \lambda_k|}{\lambda_k}. \tag{82}$$

Here $\omega_{N,k}$ is the kth natural frequency calculated using N-Tchebychev polynomials and λ_k is the corresponding natural frequency from Newton's shooting method. Obtaining spectral-Tchebychev solutions for different boundary conditions required changing only the β coefficients without need for re-derivation. It should be noted that due to the nature of projection equation of Eq. (25), the $\mathbf{z}$ is an $(N - M)$-vector where M is the number of boundary conditions. Therefore, when solving Euler–Bernoulli and Timoshenko beam problems, four polynomials are needed for satisfying the boundary conditions. Accordingly, calculation of the kth natural frequency would require a minimum of $(k + M)$ polynomials.

It is seen from Fig. 1 that, as expected, the overall convergence is approximately exponential (the ordinate in the figure is in logarithmic scale). The step-like convergence is due to the fact that Tchebychev polynomials add alternating odd and even terms with each increased number of polynomials. Thus, to increase the accuracy for an even mode (such as the first mode of the pinned–pinned case in Fig. 1(a)) or for an odd mode, two additional polynomials are required. In each case, an error less than 10^{-11} for the fifth mode is obtained by using 20 polynomials.

Another observation from Fig. 1 is that, adding more polynomials after establishing the convergence lowers the accuracy of the natural frequencies. The reason for the reduced accuracy is the poor numerical condition of the fourth-derivative matrix $\mathbf{D}^4$ for high number of polynomials. To avoid this error, minimum number of polynomials that will provide the sufficient accuracy should be selected.

Fig. 2 gives the first five mode shapes and associated (nondimensional) natural frequencies obtained for $N = 15$ Tchebychev polynomials for Euler–Bernoulli beams with different boundary conditions.

For beams with small aspect ratio, shear deformation and rotary inertia effects become important. For instance, for a cantilever beam with an aspect ratio of 5, the difference between the first three natural frequencies of Timoshenko and Euler–Bernoulli beams becomes 3%, 19%, and 40%, considering the Timoshenko beam natural frequencies as the reference.

Next, the natural frequencies of Timoshenko beams with four different boundary conditions were compared with those from Newton's shooting method. Figs. 3(a)–(d) provide the error for the first five natural

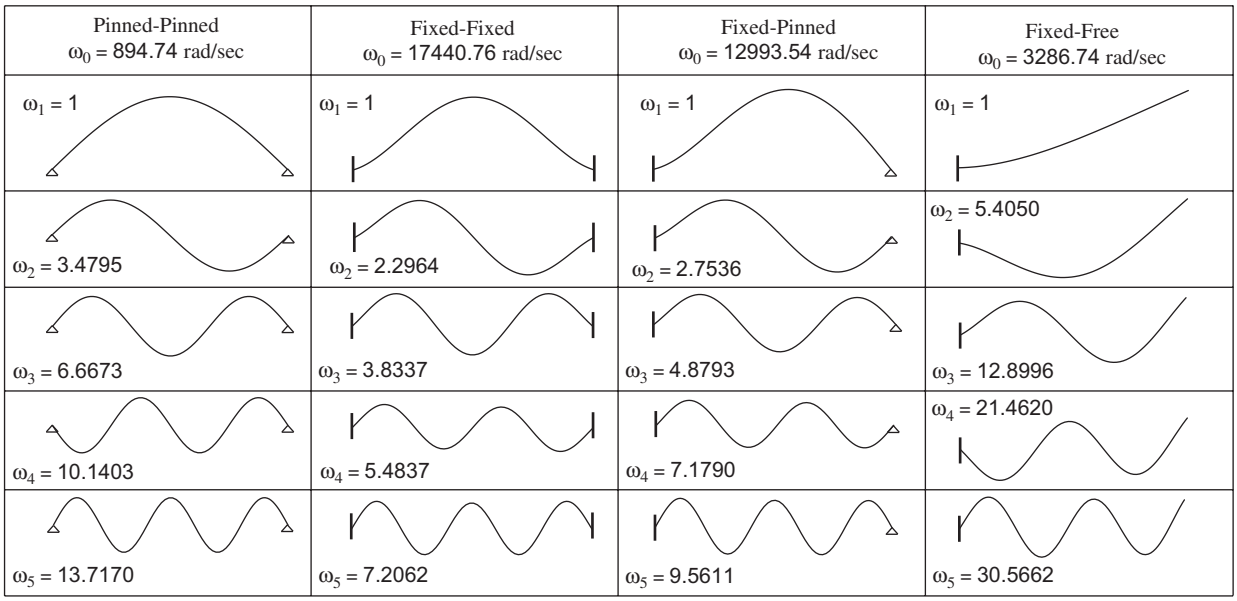

Fig. 4. First five mode shapes and normalized natural frequencies of Timoshenko beams with various boundary conditions. The natural frequencies are calculated using spectral-Tchebychev solution and normalized with respect to the first natural frequency ω_0 obtained from Newton's shooting method.

frequencies for Timoshenko beams with pinned–pinned, fixed–fixed, fixed–pinned, and fixed–free boundary conditions, respectively. In these calculations, a rectangular beam with a length of $L = 0.5\,\mathrm{m}$, a beam width of $w = 0.2\,\mathrm{m}$, a beam thickness of $h = 0.1\,\mathrm{m}$, a density of $\rho = 2300\,\mathrm{kg/m^3}$, Young's Modulus of $E = 160\,\mathrm{GPa}$, Poisson's ratio of $v = 0.25$ and a shear factor of $k_s = 0.833$ was used. Shear modulus G is calculated from $G = E/(2 + 2v)$. The error between the spectral-Tchebychev solution and Newton's method was obtained using Eq. (82).

It is seen from Fig. 3 that the convergence is very rapid. However, the convergence of higher natural frequencies is slightly slower than that of lower natural frequencies. For any of the boundary conditions, 20 polynomials provided better than 10^{-10} accuracy. In addition, unlike the case for the Euler–Bernoulli beams, increased number of polynomials did not cause degrading accuracy. This is due to the fact that the Timoshenko beam equations are only second order, and the calculation of the second-derivative matrix ($\mathbf{D}^2$) causes less numerical error at higher number of polynomials.

Fig. 4 shows the first five mode shapes of Timoshenko beams and associated natural frequencies. The natural frequencies are scaled with respect to the first natural frequency of Timoshenko beams with the same geometry and boundary conditions obtained from Newton's shooting method.

6. Application of the spectral-Tchebychev technique

To demonstrate the application of the spectral-Tchebychev technique, four different beam problems are solved. First, the modes of tapered Timoshenko beams with varying taper ratio and different boundary conditions are considered, and the natural frequencies are compared to those from Newton's shooting method. Next, a linear Euler–Bernoulli beam problem with elastic support and spatially varying sinusoidal forcing is solved. This is followed by solving two nonlinear beam problems, including an Euler–Bernoulli beam with large deflections, and a micro-beam with electrostatic forcing. For the case of the nonlinear beams, the results are compared to those from the literature.

In each case, the problems are nondimensionalized, and for the cases presented below (both linear and nonlinear), when a time integration is required due to a time-dependent forcing function, a stiff (implicit) solver (`ode15s` in Matlab®) is used. The absolute and relative tolerances for the solver are both set to 1×10^{-7}. This implicit solver is appropriate since the beam problems presented below are evolving in a time scale much longer than the time scale of the highest modes.

6.1. Dynamics of tapered Timoshenko beams

The spectral-Tchebychev technique presented here can be applied to beams with spatially varying parameters [45,46]. To demonstrate this application, the eigenvalue problem for tapered Timoshenko beams with different taper ratios and boundary conditions is solved using the spectral-Tchebychev technique. The solution is compared to those from Newton's shooting method (with 10^{-11} resolution).

Fig. 5 gives the geometry of a tapered, circular cross-section beam with the base diameter of d_0, the tip diameter d_L, and the length of L. To calculate the modes of tapered Timoshenko beams, the general Timoshenko beam equations (Eq. (57)) were used. Due to the change in cross-section along the beam length, the cross-sectional area A and the area moment of inertia I are functions of the spatial variable x. A new set of

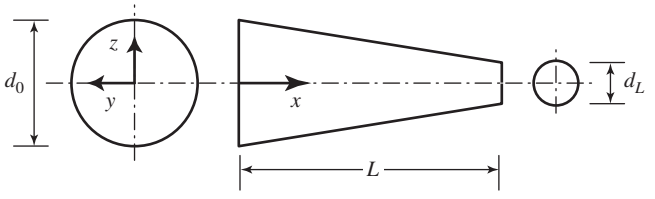

Fig. 5. The geometry of tapered Timoshenko beams.

nondimensional equations are derived considering these spatially varying parameters as

$$[A(x)(y'-\psi)]' - \chi_p A(x)\ddot{y} = f(x,t), \quad 0<x<1, \tag{83}$$

$$\sigma_p[I(x)\psi']' + A(x)(y'-\psi) - \chi_p I(x)\ddot{\psi} = \Psi(x,t), \quad 0<x<1, \tag{84}$$

where

$$x = x^*/L, \quad y = y^*/L, \quad t = t^*\omega_0, \quad \psi^* = \psi, \quad A(x) = A(x^*)/L^2, \quad I(x) = I(x^*)/L^4,$$

$$\chi_p = \frac{\rho L^2\omega_0^2}{k_s G}, \quad f = -\frac{f^*}{k_s GL}, \quad \sigma_p = \frac{E}{k_s G}, \quad \Psi = -\frac{\Psi^*}{k_s GL^2}. \tag{85}$$

To solve this problem while retaining the self-adjointness (symmetry) of the system, Galerkin's method was applied as in Eq. (43). Eqs. (73) and (74) were thus modified as

$$\boldsymbol{\theta}_y^{\mathrm{T}}[(\mathbf{V}_A\mathbf{Q}_2 + \mathbf{V}'_A\mathbf{Q}_1)\mathbf{y} - (\mathbf{V}_A\mathbf{Q}_1 + \mathbf{V}'_A)\boldsymbol{\psi} - \chi_p\mathbf{V}_A\ddot{\mathbf{y}} - \mathbf{V}\mathbf{f}] = 0, \tag{86}$$

$$\boldsymbol{\theta}_\psi^{\mathrm{T}}[\sigma_p(\mathbf{V}_I\mathbf{Q}_2 + \mathbf{V}'_I\mathbf{Q}_1)\boldsymbol{\psi} + \mathbf{V}_A(\mathbf{Q}_1\mathbf{y} - \boldsymbol{\psi}) - \chi_p\mathbf{V}_I\ddot{\boldsymbol{\psi}} - \mathbf{V}\boldsymbol{\Psi}] = 0, \tag{87}$$

where $\mathbf{V}_{\mathscr{P}}$ is the inner-product matrix associated with the parameter(s) $\mathscr{P}$. The derivatives in Eq. (83) were expanded following the chain rule, which requires the inner products of the differentiated parameters $\mathbf{V}'_{\mathscr{P}}$. This is performed as

$$\int_{\ell_1}^{\ell_2} \psi(x)\theta(x)\mathscr{P}(x)'\,\mathrm{d}x = \boldsymbol{\psi}^{\mathrm{T}}\mathbf{V}'_{\mathscr{P}}\boldsymbol{\theta}. \tag{88}$$

Differentiation $\mathscr{P}(x)'$ was computed in the spatially discretized domain using the Tchebychev differentiation as described in Eq. (13). Accordingly, the spatially discretized equations of motion become

$$\boldsymbol{\theta}^{\mathrm{T}}(\mathbf{M}_s\ddot{\mathbf{q}} + \mathbf{K}_s\mathbf{q} - \mathbf{B}_s\tilde{\mathbf{f}}) = 0, \tag{89}$$

where

$$\mathbf{q} = \begin{bmatrix}\mathbf{y}\\ \boldsymbol{\psi}\end{bmatrix}, \quad \boldsymbol{\theta} = \begin{bmatrix}\boldsymbol{\theta}_y\\ \boldsymbol{\theta}_\psi\end{bmatrix}, \quad \tilde{\mathbf{f}} = \begin{bmatrix}\mathbf{f}\\ \boldsymbol{\Psi}\end{bmatrix} \tag{90}$$

and

$$\mathbf{M}_s = -\chi_p\begin{bmatrix}\mathbf{V}_A & 0\\ 0 & \mathbf{V}_I\end{bmatrix}, \quad \mathbf{K}_s = \begin{bmatrix}(\mathbf{V}_A\mathbf{Q}_2 + \mathbf{V}'_A\mathbf{Q}_1) & -(\mathbf{V}_A\mathbf{Q}_1 + \mathbf{V}'_A)\\ \mathbf{V}_A\mathbf{Q}_1 & \sigma_p(\mathbf{V}_I\mathbf{Q}_2 + \mathbf{V}'_I\mathbf{Q}_1) - \mathbf{V}_A\end{bmatrix},$$

$$\mathbf{B}_s = \begin{bmatrix}\mathbf{V} & 0\\ 0 & \mathbf{V}\end{bmatrix}. \tag{91}$$

Table 1
Natural frequencies (rad/s) of the tapered beam from the spectral-Tchebychev solution with 20 polynomials and error with respect to Newton's shooting method calculated from Eq. (82)

	Pinned–pinned		Fixed–fixed		Fixed–pinned		Fixed–free	
	Freq.	Error	Freq.	Error	Freq.	Error	Freq.	Error
Mode 1	2256.73	2.5×10^{-10}	6359.84	7.1×10^{-10}	5566.47	1.8×10^{-10}	3212.34	7.9×10^{-11}
Mode 2	11 266.55	3.6×10^{-10}	16 758.16	1.4×10^{-9}	15 053.76	3.2×10^{-10}	9434.58	4.1×10^{-11}
Mode 3	24 452.37	4.7×10^{-10}	31 716.97	3.4×10^{-9}	29 078.93	4.8×10^{-10}	20 102.38	3.2×10^{-10}
Mode 4	41 981.44	7.7×10^{-10}	50 709.65	9.1×10^{-9}	47 228.21	8.8×10^{-10}	35 159.69	1.6×10^{-9}
Mode 5	63 400.20	1.8×10^{-10}	73 204.28	2.2×10^{-8}	69 004.32	2.2×10^{-9}	54 208.93	4.8×10^{-9}

Natural frequencies can be computed from the system matrices $\mathbf{M}_s$ and $\mathbf{K}_s$. To simulate the response to a forcing function, the state-space matrices could be formed using these system matrices as described in Eqs. (37) and (38). It should be noted here that the equations of motion given in Eq. (83) can be used for any beam with smooth uniform or nonuniform geometry, and for beams with varying material properties along the axis. If there are nonsmooth variations on the boundary, i.e., if one of the functions describing the beam geometry and material properties is not infinitely differentiable, Gibbs phenomenon will be observed [41] which deteriorates the convergence of the solution. Nonsmooth problems can be handled using a form of component

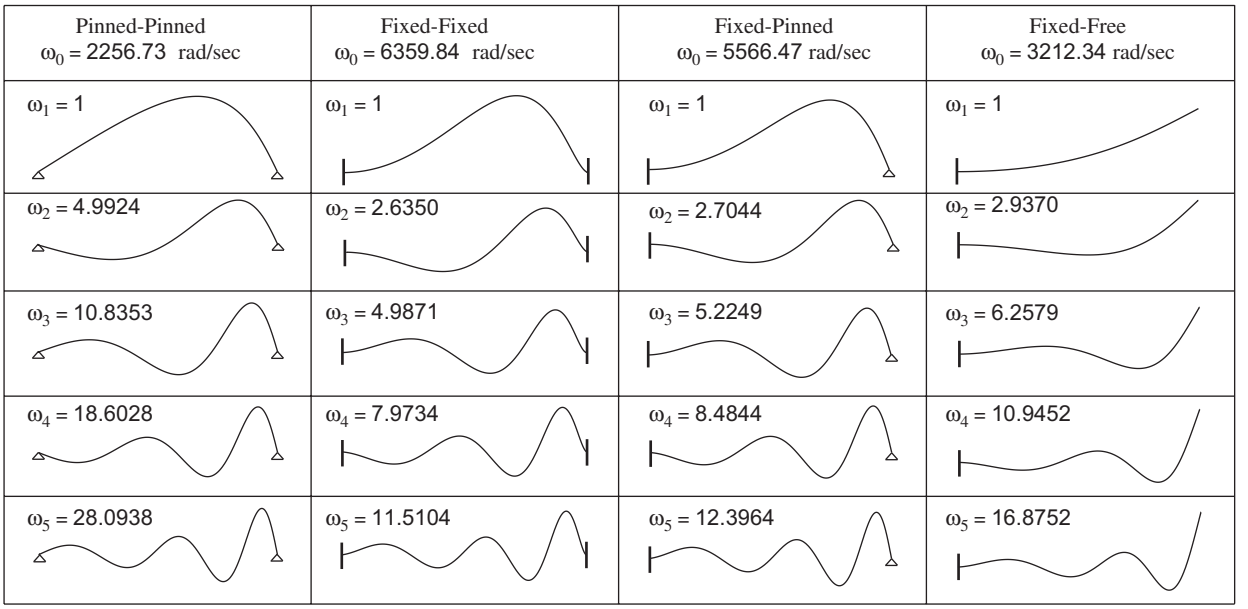

Fig. 6. First five mode shapes and normalized natural frequencies of tapered Timoshenko beams with various boundary conditions. The natural frequencies are calculated using spectral-Tchebychev solution and normalized with respect to the first natural frequency ω_0 obtained from Newton's shooting method.

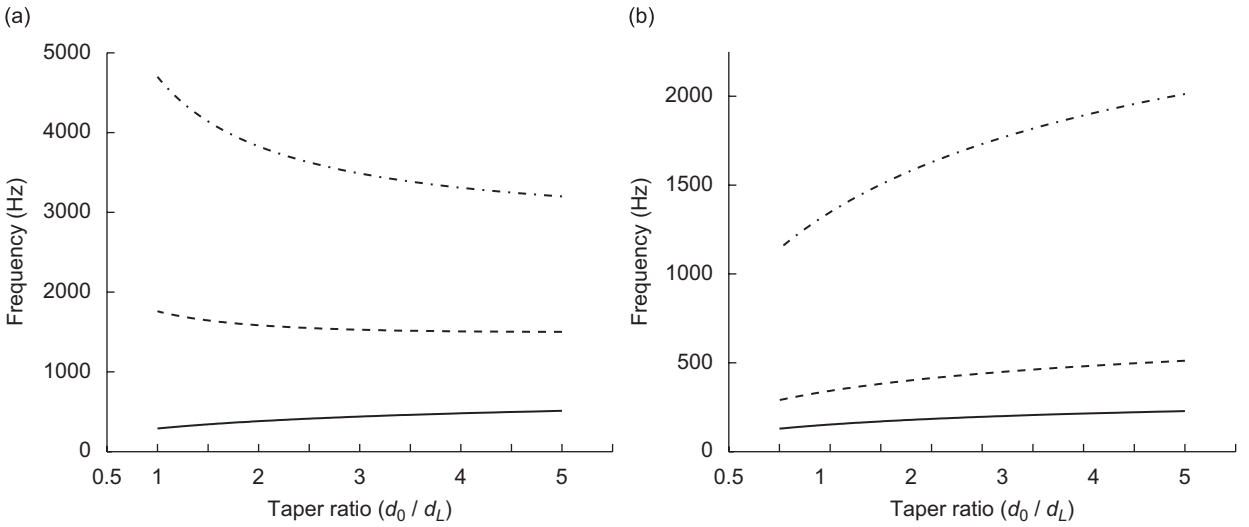

Fig. 7. (a) Change in the first three natural frequencies (ω_1 —, ω_2 - - -, ω_3 -·-) of the tapered fixed–free Timoshenko beam for varying taper ratio, (b) change in the first natural frequency of the tapered fixed–free Timoshenko beam for varying taper ratio and beam length L ($L = 0.6$ m —, $L = 0.4$ m - - -, $L = 0.2$ m -·-).

mode synthesis by defining boundaries at the locations where nonsmooth variations are present. By using the component mode synthesis, Gibbs phenomenon can be avoided and a rapid convergence is obtained.

Table 1 provides the first five natural frequencies of a tapered beam with a taper ratio of 5 for four different boundary conditions. Also given is the difference between the natural frequencies calculated from Newton's shooting method and spectral-Tchebychev solutions. The following physical parameters were used for the calculations:

$$L = 0.4\,\mathrm{m}, \quad d_0 = 0.04\,\mathrm{m}, \quad d_L = 0.008\,\mathrm{m},$$

$$E = 160\,\mathrm{GPa}, \quad \rho = 2300\,\mathrm{kg/m^3}, \quad v = 0.3, \quad k_s = 0.886. \tag{92}$$

It is seen that the error in the natural frequencies from 20 polynomials spectral-Tchebychev solution with respect to Newton's shooting method is less than 2.2×10^{-8} for any of the boundary conditions. Fig. 6 gives the mode shapes obtained from the spectral-Tchebychev technique for the tapered beams.

Various parametric analysis can be easily conducted using the numerically efficient spectral-Tchebychev solution. As an example, a study of the effect of taper ratio and tapered-beam length on the natural frequencies was performed. Fig. 7(a) gives the change in first three natural frequencies with increasing taper ratio, where the beam geometric parameters were $L = 0.4$ and $d_0 = 0.04\,\mathrm{m}$ for a fixed–free boundary condition. Fig. 7(b) gives the change in the first natural frequency with the taper ratio for three different beam lengths for the same boundary condition. Again, obtaining these solutions did not require re-derivation of the solutions.

6.2. An Euler–Bernoulli beam with elastic support and spatially varying forcing

In this section, the application of the spectral-Tchebychev technique to an Euler–Bernoulli beam with elastic boundary condition and spatially varying forcing function is demonstrated. Fig. 8 illustrates the beam and its boundary conditions.

To apply the spectral-Tchebychev technique to this problem, the boundary coefficients were set to

$$\beta_{010} = L, \quad \beta_{020} = 1, \quad \alpha_{01} = \alpha_{02} = 0,$$

$$\beta_{L12} = \frac{EI}{L}, \quad \beta_{L23} = -\frac{EI}{L^2}, \quad \beta_{L20} = -kL, \quad \alpha_{L1} = 0, \quad \alpha_{L2} = -cL\omega_0\dot{y}, \tag{93}$$

where c is the damping coefficient and k is the stiffness. All other β's were set to zero. The nondimensional forcing function $f(x,t)$ on the right-hand side of Eq. (48) was specified as

$$f(x,t) = F_0 \frac{L^3}{EI} \sin(x\pi)\sin(\omega t), \tag{94}$$

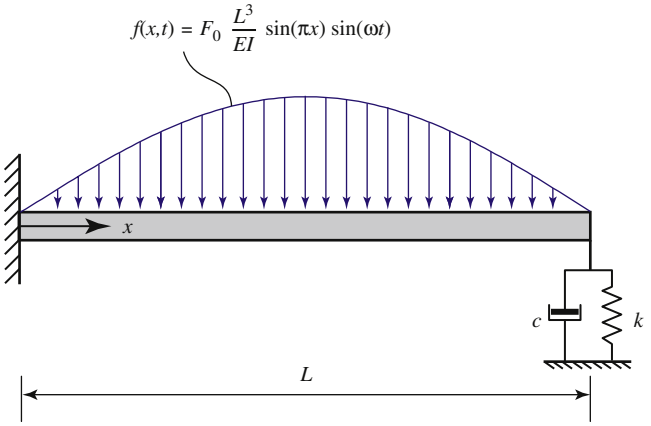

Fig. 8. An Euler–Bernoulli beam with elastic support and spatially varying forcing.

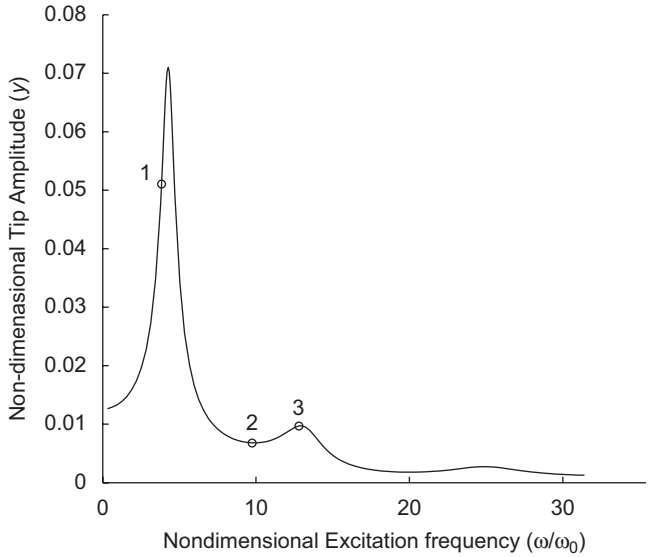

Fig. 9. The nondimensional response amplitude at the tip of the beam ($x = L$) as a function of the nondimensional excitation frequency.

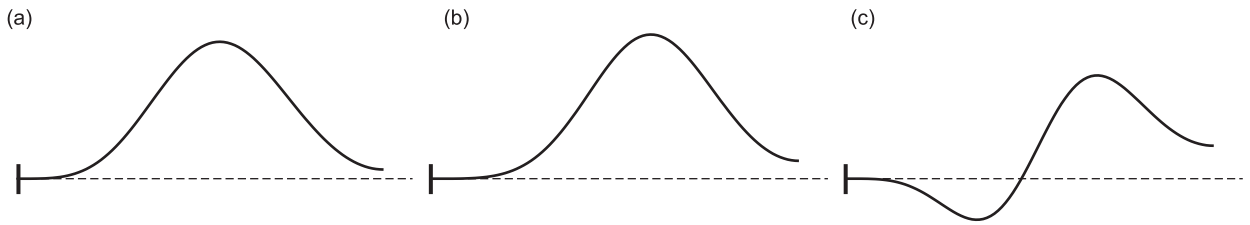

Fig. 10. Operating deflection shapes at (a) $\omega_1/\omega_0 = 3.80$, (b) $\omega_2/\omega_0 = 9.75$, and (c) $\omega_3/\omega_0 = 12.80$.

where F_0 is the force amplitude and ω is the excitation frequency. For this problem, a rectangular micro-beam with a length of $L = 500\,\mu\text{m}$, a width of $w = 18\,\mu\text{m}$, a thickness of $h = 2.25\,\mu\text{m}$, a density of $\rho = 2300\,\text{kg/m}^3$, and Young's modulus of $E = 160\,\text{GPa}$ was used. The (nondimensional) stiffness and the damping coefficients were specified as

$$k = 0.4\frac{L^3}{EI} \quad \text{and} \quad c = 0.3\frac{L^3}{EI}\omega_0. \tag{95}$$

As seen from the boundary coefficients, the damping and stiffness elements were taken into account through the boundary conditions. For the damping element, the $\dot{y}$ term was calculated at every time-integration step. Similarly, the temporal portion of the forcing function was evaluated at every integration step. On the other hand, the spatial distribution of the forcing function was considered by Gauss–Lobatto sampling as

$$\mathbf{f} = \frac{L^3}{EI}F_0\mathbf{f}_s \sin\omega t, \tag{96}$$

where $\mathbf{f}_s$ is the spatially sampled part of the forcing function.

Fig. 9 gives the nondimensional response amplitude at $x = L$ as a function of the nondimensional excitation frequency. The first natural frequency of the fixed–free beam ($\omega_0 = 76190.13\,\text{rad/s}$) was used to nondimensionalize the excitation frequency and the time. In Fig. 10, the operating deflection shapes at three frequencies ((a) $\omega_1/\omega_0 = 3.80$, (b) $\omega_2/\omega_0 = 9.75$, (c) $\omega_3/\omega_0 = 12.80$) are given at the instant when the maximum tip displacement is reached. The nondimensional tip response is given as a function of nondimensional time for the same three frequencies in Fig. 11. It is seen that the spectral-Tchebychev

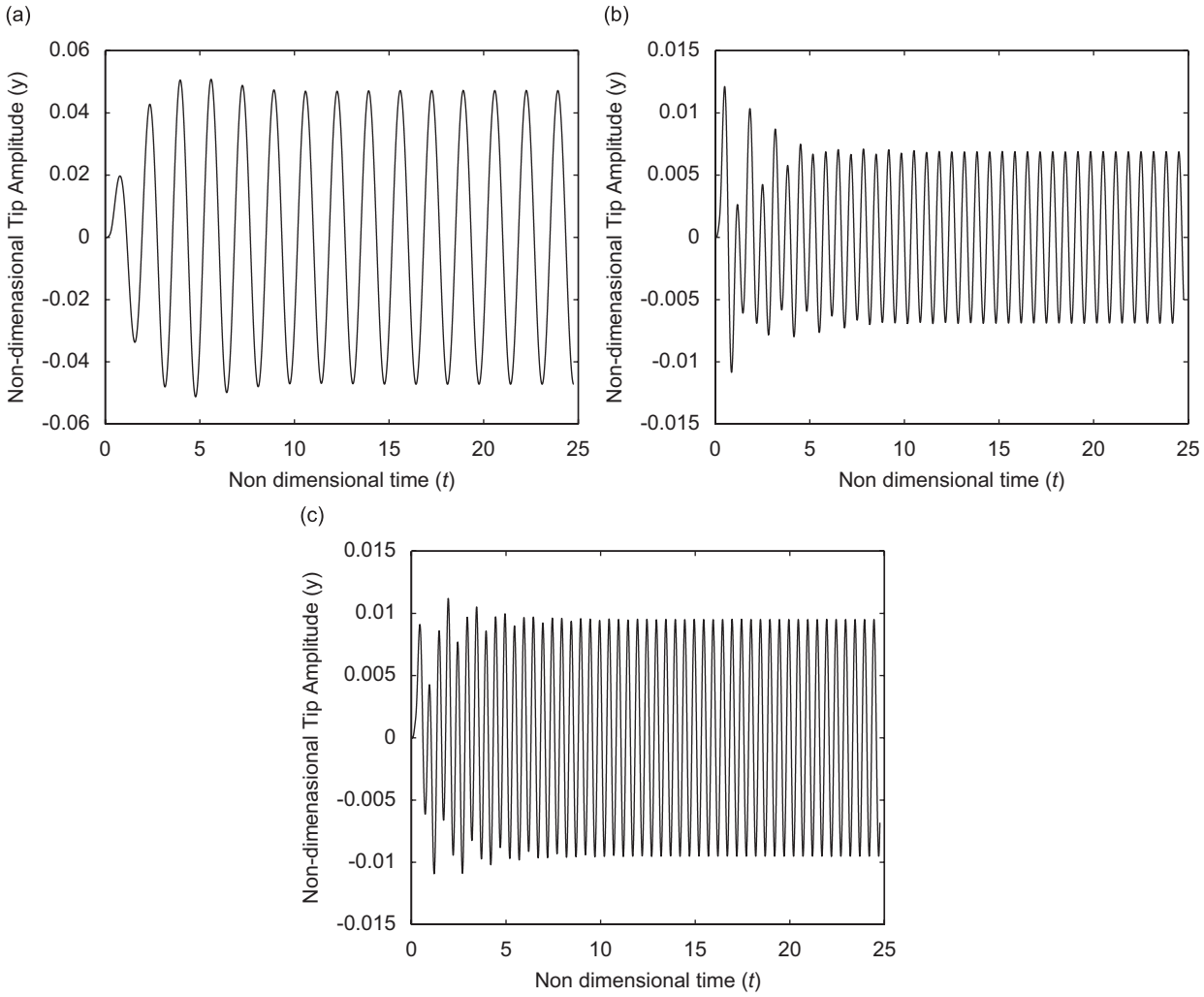

Fig. 11. Time responses at (a) $\omega_1/\omega_0 = 3.80$, (b) $\omega_2/\omega_0 = 9.75$, and (c) $\omega_3/\omega_0 = 12.80$.

technique can effectively simulate such a problem with elastic boundary condition, damping, and spatially and temporally varying forcing function.

6.3. Nonlinear behavior of a large-deflection Euler–Bernoulli beam with immovable ends

To demonstrate the applicability of spectral-Tchebychev technique to nonlinear beams, the nonlinear behavior of an Euler–Bernoulli beam with immovable ends is considered for different boundary conditions. The results were compared with those given in Ref. [47] for a combined modal/finite element solution.

For a beam with immovable ends, the length of the beam has to increase to accommodate the deflection of the beam. When the beam is subjected to deflections larger than the beam thickness, the forces arising from this stretching effect induce nonlinear behavior. Many researchers studied this problem using analytical (e.g., Refs. [48,49]), perturbation (e.g., Ref. [50]), variational (e.g., Ref. [51]), Galerkin (e.g., Refs. [19,52]), and finite element (e.g., Refs. [47,53,54]) methods.

The nonlinear boundary-value problem for large-deflection Euler–Bernoulli beam with uniform geometry can be written as [48]

$$m\ddot{y} + y'''' - (S_0 + S_1)y'' = f \quad (0 \leqslant x \leqslant 1), \tag{97}$$

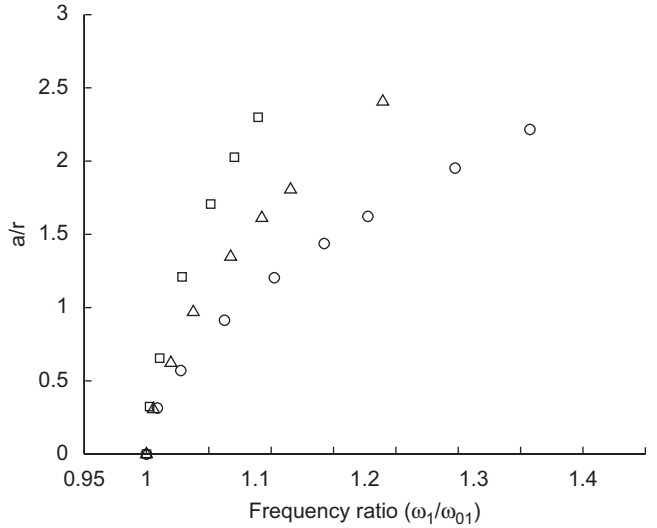

Fig. 12. Change in the frequency ratio with steady-state response amplitude for three general boundary condition types (fixed–fixed —, fixed–pinned - - -, pinned–pinned ---).

where m and f are defined in Eq. (50), and

$$S_0 = \frac{P_0 L^2}{EI}, \quad S_1 = \frac{AL^2}{2I}\int_0^1 (y')^2 \, \mathrm{d}x. \tag{98}$$

Here, S_1 is the nondimensional axial stretching force, and P_0 is the axial force applied to the beam. S_0 is the nondimensional form of the axial force P_0.

Applying the Gauss–Lobatto sampling and Tchebychev derivatives and definite integration, the spatially discretized form of Eq. (97) can be given as

$$m\ddot{\mathbf{y}} + \mathbf{Q}_4\mathbf{y} - (S_0 + \mathbf{S}_1)\mathbf{Q}_2\mathbf{y} = \mathbf{f}, \tag{99}$$

where

$$\mathbf{S}_1 = \frac{AL^2}{2I}\mathbf{v}^{\mathrm{T}}\boldsymbol{\Gamma}_F(\mathbf{y}')^2. \tag{100}$$

Here, $\mathbf{v}$ is the definite integral vector given in Eq. (14). Substitution of projection in Eq. (25) and application of Galerkin's method to Eq. (99) results in

$$\ddot{\mathbf{z}} = -\mathbf{M}_z^{-1}\mathbf{K}_z\mathbf{z} - \mathbf{M}_z^{-1}\mathbf{M}_\alpha\ddot{\boldsymbol{\alpha}} - \mathbf{M}_z^{-1}\mathbf{K}_\alpha\boldsymbol{\alpha} + \mathbf{M}_z^{-1}\mathbf{B}\mathbf{f}, \tag{101}$$

where

$$\mathbf{M}_z = m\mathbf{P}^{\mathrm{T}}\mathbf{V}\mathbf{P}, \quad \mathbf{K}_z = \mathbf{P}^{\mathrm{T}}[\mathbf{V}\mathbf{Q}_4 - (S_0 + \mathbf{S}_1)\mathbf{V}\mathbf{Q}_2]\mathbf{P},$$

$$\mathbf{M}_\alpha = m\mathbf{P}^{\mathrm{T}}\mathbf{V}\mathbf{R}, \quad \mathbf{K}_\alpha = \mathbf{P}^{\mathrm{T}}[\mathbf{V}\mathbf{Q}_4 - (S_0 + \mathbf{S}_1)\mathbf{V}\mathbf{Q}_2]\mathbf{R}, \quad \mathbf{B} = \mathbf{P}^{\mathrm{T}}\mathbf{V}. \tag{102}$$

It can be seen that the stiffness matrix $\mathbf{K}_z$ and the forcing term $\mathbf{K}_\alpha$ depend on the stretching force $\mathbf{S}_1$. When simulating this problem, the stretching force and $\mathbf{K}_z$ and $\mathbf{K}_\alpha$ were calculated at every integration step.

In nonlinear beam problems, the ratio of the first fundamental frequency of the nonlinear beam to the first natural frequency of the corresponding linear beam changes with the steady-state amplitude. The first fundamental frequency of the nonlinear beam is the frequency for which the maximum steady-state amplitude is reached (similar to the case in Fig. 15). Fig. 12 shows the change in the ratio of the first fundamental frequency of the nonlinear beam to the first natural frequency of the corresponding linear beam with increased ratio of the steady-state response amplitude a to the radius of gyration r for three different boundary

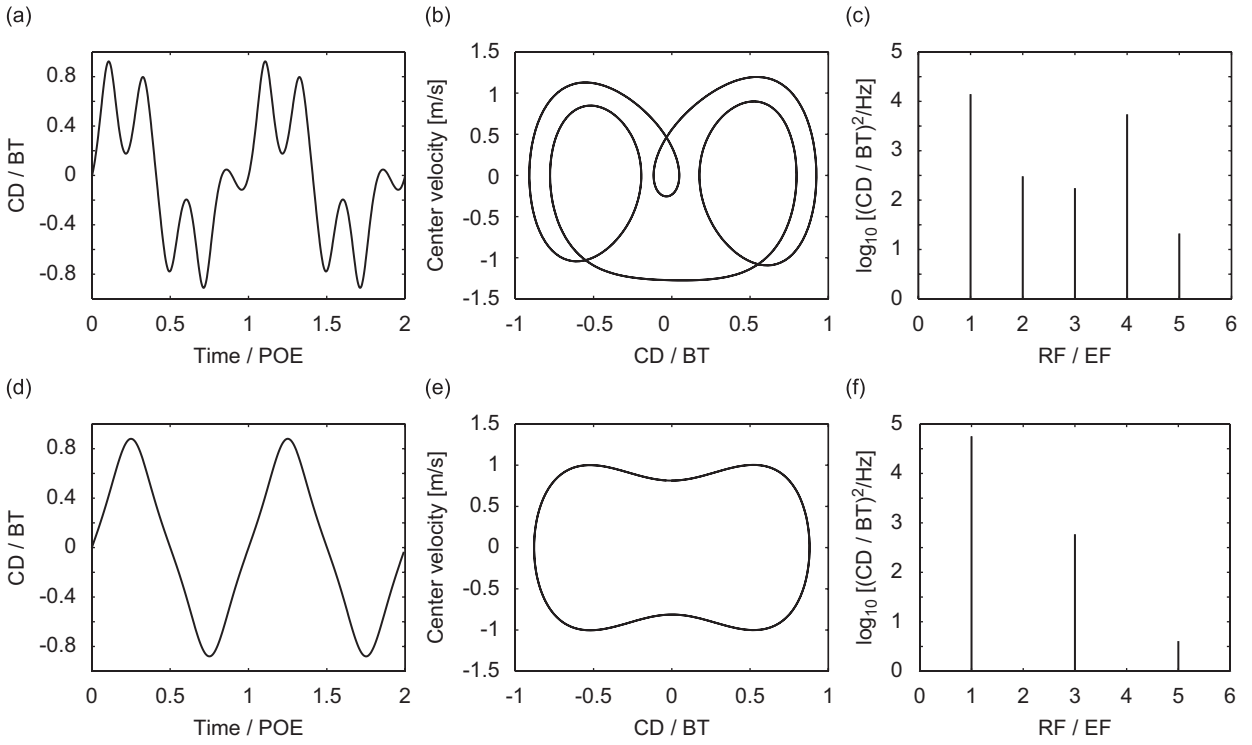

Fig. 13. (a)–(c) Time response, phase diagram and power spectral density, respectively, for a pinned–pinned beam (case 1), (d)–(e) time response, phase diagram and power spectral density, respectively, for a pinned–pinned beam (case 2) (CD—center displacement, BT—beam thickness, POE—period of excitation, RF—response frequency, EF—excitation frequency, PSD—power spectral density).

conditions. For this problem, the constant axial force S_0 and the external force f were set to zero. It is seen that the increased steady-state response amplitude increases the natural frequency. This trend closely matches that in Ref. [54].

As another example, the harmonic response of the large-deflection Euler–Bernoulli beam was considered. A forcing function with uniform spatial distribution and with a time-dependent amplitude as

$$f^* = F_0 \sin(2\pi f_e t^*) \tag{103}$$

was applied to the beam. During the simulation, the forcing function was evaluated at every integration step. Fig. 13 shows the time domain response, phase graph, and power spectral density at two different excitation frequencies ($f_{e1} = 10\,\text{Hz}$ and $f_{e2} = 22.5\,\text{Hz}$) for a pinned–pinned beam with $F_0 = 500\,\text{N/m}$. The same plots are given in Fig. 14 for a fixed–fixed beam at $f_{e1} = 18.75\,\text{Hz}$ and $f_{e2} = 105\,\text{Hz}$ and with $F_0 = 1000\,\text{N/m}$. Furthermore, Fig. 15 gives the change in response amplitude with the frequency, and shows the well-known jump phenomenon. Beam parameters given in Ref. [47] were used in the analysis and the results presented here correspond to those given in Ref. [47]; the agreement between the spectral-Tchebychev results and those from Ref. [47] is excellent.

6.4. A micro-beam with electrostatic excitation

In this section, the application of the spectral-Tchebychev technique to modeling a micro-beam with electrostatic excitation is demonstrated. Electrostatic excitation is a common technique used for micro-electromechanical systems (MEMS) [55]. Beams with electrostatic excitation are utilized in various sensors and actuators. The electrostatic force depends nonlinearly on the dynamic gap between the beam and the electrode on the substrate. Therefore, the response of the micro-beams under electrostatic excitation is nonlinear.

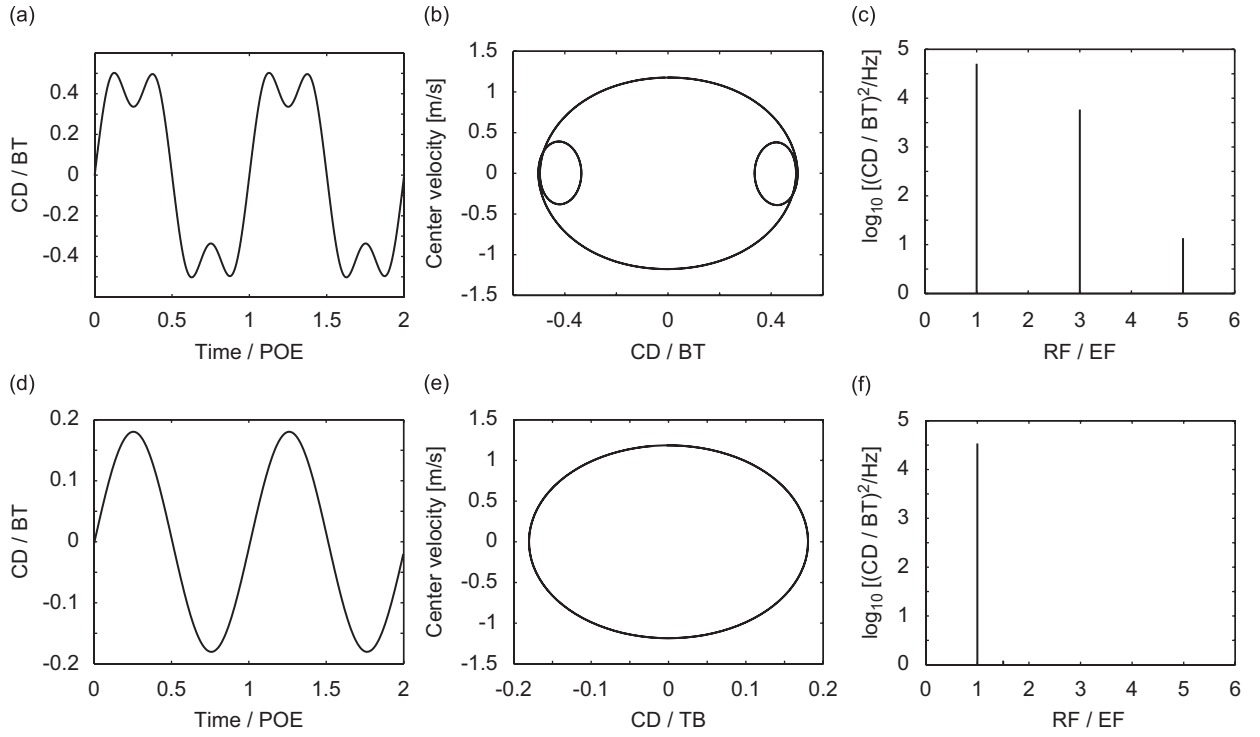

Fig. 14. (a)–(c) Time response (CD—center displacement, BT—beam thickness), phase diagram and power spectral density, respectively, for a fixed–fixed beam (case 1), (d)–(e) time response, phase diagram and power spectral density, respectively, for a fixed–fixed beam (case 4).

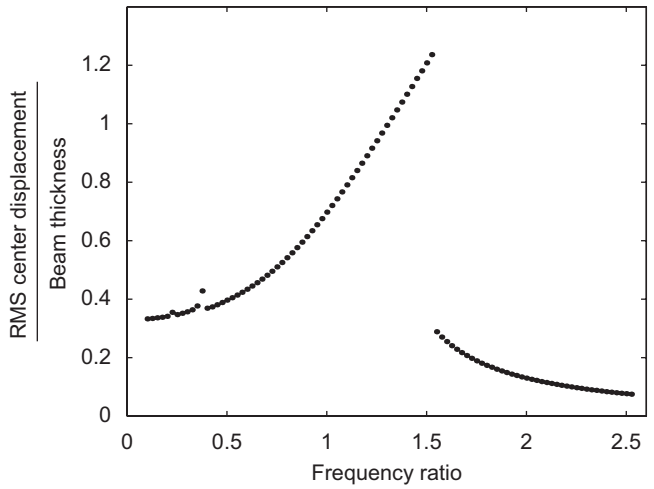

Fig. 15. Frequency response of the fixed–fixed large-amplitude beam simulated in Ref. [47].

An Euler–Bernoulli beam with electrostatic excitation, stretching force, and damping (arising from the gas surrounding the micro-beam) can be given as

$$m\ddot{y} + c\dot{y} + y'''' - (S_0 + S_1)y'' = f_s(x,t) \quad (0 \leqslant x \leqslant 1), \tag{104}$$

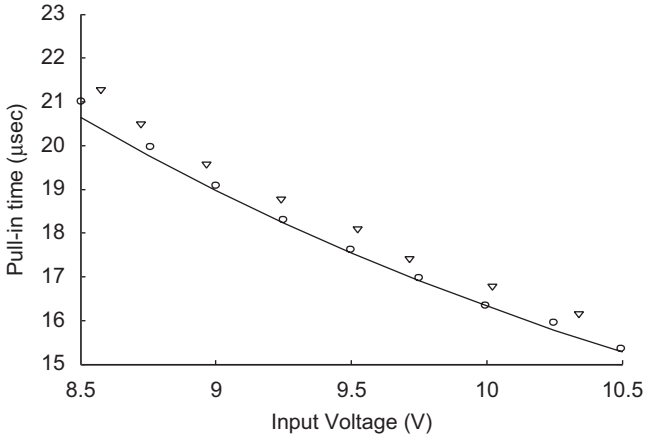

Fig. 16. The pull-in time for the pressure sensor. The inverted triangles and the circles are from experiments and numerical solutions in Ref. [56], respectively. The solid line is the solution obtained from the spectral-Tchebychev technique.

where

$$c = \frac{c^* L^4 \omega_0}{EI}, \quad f_s(x,t) = \varepsilon_0 b \frac{2V_a^2}{(g_0 - y)^2} \frac{L}{EI}. \tag{105}$$

Here c^* is the damping coefficient per unit length, ε_0 is the permittivity constant, b is the beam thickness, V_a is the applied voltage, and g_0 is the initial gap between the beam and the substrate.

When voltages greater than the so-called pull-in voltage are supplied, the beam collapses onto the substrate electrode. The time it takes between the voltage application and occurrence of pull-in is highly sensitive to the ambient pressure. This problem was studied by Hung and Senturia [56], where the experimental and modeling results were shown to agree. They used Galerkin's method with basis functions obtained from finite element solution to model the nonlinear behavior of the beam.

In solving this problem using the spectral-Tchebychev technique, Eq. (104) is spatially discretized using Gauss–Lobatto sampling and Tchebychev derivatives and integrations as

$$m\ddot{\mathbf{y}} + c\dot{\mathbf{y}} + \mathbf{Q}_4\mathbf{y} - (S_0 + \mathbf{S}_1)\mathbf{Q}_2\mathbf{y} = \mathbf{F}_s. \tag{106}$$

The terms $\mathbf{S}_1$, and $\mathbf{F}_s$ are computed at every time-integration step for each Gauss–Lobatto points.

The dependence of pull-in time on the ambient pressure is given in Fig. 16. The figure shows the experimental data and the results from Ref. [56], as well as the results of the spectral-Tchebychev model using the same parameters and boundary conditions as in Ref. [56]. The spectral-Tchebychev model matches very closely with the results from both the experimentation and the model of Hung and Senturia.

7. Summary and conclusions

This paper presented a new spectral-Tchebychev technique for solving linear and nonlinear beam problems. The technique uses orthogonal Tchebychev polynomials as basis functions, and applies Galerkin's method to obtain the solution. After describing the properties of the Tchebychev polynomials and associated series expansion, the derivation of the solution for the wave equation, the Euler–Bernoulli beam problem, and the Timoshenko beam problem was outlined. For self-adjoint problems, the system matrices obtained from the spectral-Tchebychev technique were symmetric, indicating that the technique is equivalent to the variational approaches for self-adjoint problems. This is an important property that insures the numerical robustness of the spectral-Tchebychev technique.

The numerical accuracy and convergence characteristics of the technique were studied by solving eigenvalue problems for Euler–Bernoulli and Timoshenko beams with different boundary conditions, and comparing the

modes to those from Newton's shooting method. It was seen that the convergence is exponential, and only a small number of polynomials is sufficient to obtain the machine-precision accuracy.

The application of the technique was then demonstrated on two linear problems. First, the natural frequencies and the mode shapes of a tapered Timoshenko beam with different boundary conditions were determined with the spectral-Tchebychev technique. The solution was compared with Newton's shooting method and it was observed that machine precision accuracy was obtained. Next, an Euler–Bernoulli beam with spatially and temporally varying forcing function, elastic boundary, and damping was analyzed.

Two nonlinear problems from the literature were also considered to demonstrate the effectiveness of the solution. The first problem included a large-deflection Euler–Bernoulli beam with different boundary conditions. The second problem included a micro-beam with (nonlinear) electrostatic excitation and stretching force. For both cases, the solutions obtained using the spectral-Tchebychev technique were in an excellent agreement with those from the literature.

In conclusion, the spectral-Tchebychev technique derived here is a numerically efficient and accurate approximate solution applicable to a wide range of linear, nonlinear, self-adjoint, and nonself-adjoint beam problems. Furthermore, the solution can be applied to beams with nonuniformly varying parameters and different boundary conditions without need for re-derivation.

Acknowledgments

This work was supported in part by Sandia National Laboratories. Sandia is a multiprogram laboratory operated by Sandia Corporation, a Lockheed Martin Company, for the United States Department of Energy under contract DE-AC04-94AL85000. This work was funded in part by the National Science Foundation CAREER program CMII-0547534 (Ozdoganlar).

Appendix A. Forward and backward transform matrices

Consider the truncated Tchebychev expansion of a function $y(x)$,

$$y(x) = \sum_{k=0}^{N-1} a_k \mathscr{T}_k(x). \tag{A.1}$$

Let $\{x_j\}_{j=1}^{N}$ be N scaled Gauss–Lobatto points (see Eq. (8)). Evaluating (A.1) at these points

$$\begin{bmatrix} y_0 \\ y_1 \\ \vdots \\ y_{N-1} \end{bmatrix} = \begin{bmatrix} \mathscr{T}_0(x_0) & \mathscr{T}_1(x_0) & \mathscr{T}_2(x_0) & \cdots & \mathscr{T}_{N-1}(x_0) \\ \mathscr{T}_0(x_2) & \mathscr{T}_1(x_1) & \mathscr{T}_2(x_1) & \cdots & \mathscr{T}_{N-2}(x_1) \\ \vdots & \vdots & \vdots & \ddots & \vdots \\ \mathscr{T}_0(x_{N-1}) & \mathscr{T}_1(x_{N-1}) & \mathscr{T}_2(x_{N-1}) & \cdots & \mathscr{T}_{N-1}(x_{N-1}) \end{bmatrix} \begin{bmatrix} a_0 \\ a_1 \\ \vdots \\ a_{N-1} \end{bmatrix}. \tag{A.2}$$

Here, the $N \times N$ coefficient matrix on the right-hand side is the *backward* transform matrix $\mathbf{\Gamma}_B$. It follows from Eq. (7) that $\mathbf{\Gamma}_F = \mathbf{\Gamma}_B^{-1}$.

Appendix B. Differentiation matrix

The derivative of each Tchebychev polynomial can be recursively expressed in terms of lower-order Tchebychev polynomials (see Eq. (11)). Using the recursive relations, the differentiation matrix $\mathbb{D}$ defined on $(-1, 1)$ can be calculated from

$$T_0'(x) = 0, \tag{B.1}$$

$$T_1'(x) = T_0(x), \tag{B.2}$$

$$T_2'(x) = 4T_1(x), \tag{B.3}$$

$$T'_{2k-1}(x) = \sum_{m=1}^{k-1} 2(2k-1)T_{2m} + (2k-1)T_0(x), \quad k>1, \tag{B.4}$$

$$T'_{2k}(x) = \sum_{m=1}^{k} 4kT_{2m-1}, \quad k>1. \tag{B.5}$$

The differentiation matrix $\mathbf{D}$ defined on (ℓ_1, ℓ_2) is given by $\mathbf{D} = 2/(\ell_2 - \ell_1)\mathbb{D}$.

Appendix C. Definite integral matrix

The integral of a scaled Tchebychev polynomial can be given as

$$\int_{\ell_1}^{\ell_2} \mathscr{T}_k(x)\,\mathrm{d}x = \begin{cases} \dfrac{2}{1-k^2}\dfrac{\ell_2-\ell_1}{2}, & k \text{ odd}, \\ 0, & k \text{ even}. \end{cases} \tag{C.1}$$

Thus for a function $f = \sum_{k=0}^{N} a_k \mathscr{T}_k(x)$, the definite integral can be computed as

$$\int_{\ell_1}^{\ell_2} f(x)\,\mathrm{d}x = \sum_{k=0}^{N} a_k \int_{\ell_1}^{\ell_2} \mathscr{T}_k(x)\,\mathrm{d}x = \mathbf{v}^{\mathrm{T}}\mathbf{a}. \tag{C.2}$$

Here the kth element of the vector $\mathbf{v}$ introduced in Eq. (14) is given by $\{\mathbf{v}\}_k = \int_{\ell_1}^{\ell_2} \mathscr{T}_k(x)\,\mathrm{d}x$.

Appendix D. Inner-product matrix

Let $\mathbf{f}_N$ and $\mathbf{g}_N$ are values of the functions $f(x)$ and $g(x)$ at N Gauss–Lobatto points. Since the product of interpolated functions have order $2N$, the N vectors $\mathbf{f}_N$ and $\mathbf{g}_N$ are interpolated to have $2N$ points

$$\mathbf{f}_{2N} = \mathbf{S}_2\mathbf{f}_N. \tag{D.1}$$

Here $\mathbf{S}_2 = \mathbf{\Gamma}_{B_{2N}}[\mathbb{I}_N; \mathbb{O}_N]\mathbf{\Gamma}_{F_N}$, where $\mathbf{\Gamma}_{B_{2N}}$ is the $2N \times 2N$ dimensional backward transform matrix, $\mathbb{I}_N$ and $\mathbb{O}_N$ are the $N \times N$ dimensional identity and zero matrices, respectively. Let the matrix $\mathbf{f}_{d,2N}$ has the values of $\mathbf{f}_{2N}$ at its diagonal, then the values of the product $h(x) = f(x)g(x)$ at $2N$ Gauss–Lobatto points are given by

$$\mathbf{h}_{2N} = \mathbf{f}_{d,2N}\mathbf{g}_{2N}.$$

The inner product between $f(x)$ and $g(x)$ is calculated using the definite integral vector $\mathbf{v}_{2N}$

$$\begin{aligned} \int_{\ell_1}^{\ell_2} h(x)\,\mathrm{d}x &= \mathbf{v}_{2N}^{\mathrm{T}}\mathbf{\Gamma}_{F_{2N}}\mathbf{f}_{d,2N}\mathbf{g}_{2N} \\ &= \mathbf{f}_{2N}^{\mathrm{T}}\mathbf{v}_{d,2N}\mathbf{g}_{2N}. \end{aligned} \tag{D.2}$$

Here $\mathbf{v}_{d,2N}$ is a diagonal matrix that has the values of $\mathbf{v}_{2N}^{\mathrm{T}}\mathbf{\Gamma}_{F_{2N}}$ at its diagonal. Equivalently,

$$\int_{\ell_1}^{\ell_2} h(x)\,\mathrm{d}x = \mathbf{f}_N^{\mathrm{T}}\mathbf{V}\mathbf{g}_N, \tag{D.3}$$

where the inner-product matrix $\mathbf{V} = \mathbf{S}_2^{\mathrm{T}}\mathbf{v}_{d,2N}\mathbf{S}_2$.

The inner-product matrix is slightly different when the differential equation has variable coefficients. In this case a weighted inner product is defined with the variable coefficient being the weighting function. Considering the functions $f(x)$ and $g(x)$, and the weighting function $\gamma(x)$, a similar approach is used to obtain the inner product. All functions $f(x)$, $g(x)$, and $\gamma(x)$ are assumed to be expanded using N-Tchebychev polynomials. Let $\mathbf{f}_N$, $\mathbf{g}_N$, and $\boldsymbol{\gamma}_N$ be the values of the corresponding function at N Gauss–Lobatto points. The product of Tchebychev expansion of three functions has an order of $3N$. The values of the functions at N Gauss–Lobatto

points are extrapolated to $3N$ points to better approximate the inner product such that

$$\mathbf{f}_{3N} = \mathbf{S}_3 \mathbf{f}_N. \tag{D.4}$$

Here, $\mathbf{S}_3 = \mathbf{\Gamma}_{B_{3N}}[\mathbb{I}_N; \mathbb{O}_N; \mathbb{O}_N]\mathbf{\Gamma}_{F_N}$. The product $f(x)g(x)\gamma(x)$ at $3N$ Gauss–Lobatto points is given by

$$\mathbf{h}_{3N} = \mathbf{f}_{d,3N}\boldsymbol{\gamma}_{d,3N}\mathbf{g}_{3N}, \tag{D.5}$$

where $\mathbf{f}_{d,3N}$ and $\boldsymbol{\gamma}_{d,3N}$ are $3N \times 3N$ matrices that have the values of $\mathbf{f}_{3N}$ and $\boldsymbol{\gamma}_{3N}$ at their diagonals, respectively. Using this, the weighted inner product between $f(x)$ and $g(x)$ is defined as

$$\int_{\ell_1}^{\ell_2} f(x)g(x)\gamma(x)\,\mathrm{d}x = \mathbf{f}_N^{\mathrm{T}}\mathbf{V}_\gamma \mathbf{g}_N, \tag{D.6}$$

where $\mathbf{V}_\gamma = \mathbf{S}_3^{\mathrm{T}}\mathbf{v}_{d,3N}\boldsymbol{\gamma}_{d,3N}\mathbf{S}_3$.

Appendix E. Symmetric mass and stiffness matrices

To prove the symmetry of $\mathbf{M}$ and $\mathbf{K}$ matrices of Eqs. (17) and (18), the self-adjointness of the stiffness operator is stated as

$$\int_{\ell_1}^{\ell_2} \psi_1(x)\mu\psi_2''(x)\,\mathrm{d}x = \int_{\ell_1}^{\ell_2} \psi_2(x)\mu\psi_1''(x)\,\mathrm{d}x, \tag{E.1}$$

where $\psi_1(x)$ and $\psi_2(x)$ are two functions that satisfy the homogeneous boundary conditions. If $\psi_1(x)$ and $\psi_2(x)$ are expressible *exactly* with N-Tchebychev polynomials, considering that they satisfy the homogeneous boundary conditions, they can be written in the spatially discretized space as $\mathbf{P}\boldsymbol{\psi}_1$ and $\mathbf{P}\boldsymbol{\psi}_2$, where $\mathbf{P}$ is the projection matrix given in Eq. (25). Therefore, the inner products in Eq. (E.1) can be written as

$$\int_{\ell_1}^{\ell_2} \psi_1(x)\mu\psi_2''(x)\,\mathrm{d}x = \boldsymbol{\psi}_1^{\mathrm{T}}\mathbf{P}^{\mathrm{T}}\mathbf{V}\mathbf{Q}_2\mathbf{P}\boldsymbol{\psi}_2 = \boldsymbol{\psi}_1^{\mathrm{T}}\mathbf{K}\boldsymbol{\psi}_2, \tag{E.2}$$

$$\int_{\ell_1}^{\ell_2} \psi_2(x)\mu\psi_1''(x)\,\mathrm{d}x = \boldsymbol{\psi}_2^{\mathrm{T}}\mathbf{P}^{\mathrm{T}}\mathbf{V}\mathbf{Q}_2\mathbf{P}\boldsymbol{\psi}_1 = \boldsymbol{\psi}_2^{\mathrm{T}}\mathbf{K}\boldsymbol{\psi}_1. \tag{E.3}$$

These inner products are calculated exactly since the derivative matrix $\mathbf{Q}_2$ and inner-product matrix $\mathbf{V}$ are calculated exactly for functions expressible by Tchebychev polynomials. Eqs. (E.1) and (E.2) entail

$$\boldsymbol{\psi}_1^{\mathrm{T}}\mathbf{K}\boldsymbol{\psi}_2 = \boldsymbol{\psi}_2^{\mathrm{T}}\mathbf{K}\boldsymbol{\psi}_1, \tag{E.4}$$

which can be true only if $\mathbf{K} = \mathbf{K}^{\mathrm{T}}$, i.e., $\mathbf{K}$ is symmetric. A similar approach can be followed to prove that the mass matrix $\mathbf{M}$ is also symmetric. Mass and stiffness matrices of more general problems, including problems with variable coefficients, and the various types of beam problems can be shown to be symmetric using this approach.

Appendix F. Projection matrices (basis recombination)

Consider a spatially discretized boundary value problem with the differential equation

$$L\mathbf{y} = \mathbf{f}, \tag{F.1}$$

where L is the differential operator, and the boundary conditions

$$\boldsymbol{\beta}\mathbf{y} = \alpha. \tag{F.2}$$

All $\mathbf{y}$'s that satisfy Eq. (F.2) can be given by

$$\mathbf{y} = \mathbf{w} + \mathbf{q}. \tag{F.3}$$

Here $\mathbf{w}$ is a vector in the null space of $\boldsymbol{\beta}$, and $\mathbf{q}$ is the unique vector in the null-perpendicular space of $\boldsymbol{\beta}$ such that $\boldsymbol{\beta}\mathbf{q} = \boldsymbol{\alpha}$. The null and null-perpendicular spaces can be found by using the singular value decomposition of $\boldsymbol{\beta}$. Setting $\boldsymbol{\beta} = \mathscr{U}\mathbf{S}\mathscr{V}^{\mathrm{T}}$, where $\mathscr{U}$ and $\mathscr{V}$ are unitary matrices and $\mathbf{S}$ is a matrix with the singular values of $\boldsymbol{\beta}$ in its

diagonal, the unique $\mathbf{q}$ can be determined using Eq. (F.2) as

$$\mathscr{U}\mathbf{S}\mathscr{V}^{\mathrm{T}}\mathbf{q} = \boldsymbol{\alpha}, \tag{F.4}$$

$$\mathbf{S}\mathscr{V}^{\mathrm{T}}\mathbf{q} = \mathscr{U}^{\mathrm{T}}\boldsymbol{\alpha}, \tag{F.5}$$

$$\mathbf{S}\mathbf{S}^{\mathrm{T}}\mathbf{w}_2 = \mathscr{U}^{\mathrm{T}}\boldsymbol{\alpha}, \tag{F.6}$$

$$\mathbf{w}_2 = (\mathbf{S}\mathbf{S}^{\mathrm{T}})^{-1}\mathscr{U}^{\mathrm{T}}\boldsymbol{\alpha}, \tag{F.7}$$

$$\mathbf{w}_1 = \mathbf{S}^{\mathrm{T}}(\mathbf{S}\mathbf{S}^{\mathrm{T}})^{-1}\mathscr{U}^{\mathrm{T}}\boldsymbol{\alpha}, \tag{F.8}$$

$$\mathbf{q} = \mathbf{R}\boldsymbol{\alpha}. \tag{F.9}$$

In the above relations, $\mathbf{w}_1 = \mathscr{V}^{\mathrm{T}}\mathbf{q}$, $\mathbf{w}_1 = \mathbf{S}^{\mathrm{T}}\mathbf{w}_2$, and $\mathbf{R} = \mathscr{V}\mathbf{S}^{\mathrm{T}}(\mathbf{S}\mathbf{S}^{\mathrm{T}})^{-1}\mathscr{U}^{\mathrm{T}}$.

The left singular vectors that correspond to zero singular values span the null space of $\boldsymbol{\beta}$. $\mathscr{V}$ is a matrix with N columns

$$\mathscr{V} = [v_1 \;\; v_2 \;\; \cdots \;\; v_N]. \tag{F.10}$$

Since, in the case of wave equation, rank of $\boldsymbol{\beta}$ is 2, the columns of $\mathbf{P} = [v_3 \;\; v_4 \;\; \cdots \;\; v_N]$ span the null span of $\boldsymbol{\beta}$. In this case, for an arbitrary vector $\mathbf{z}$, $\mathbf{w} = \mathbf{P}\mathbf{z}$. The particular $\mathbf{z}$ that also satisfies the algebraic equation (F.1) is the solution. Rewriting Eq. (F.3)

$$\mathbf{y} = \mathbf{P}\mathbf{z} + \mathbf{R}\boldsymbol{\alpha}. \tag{F.11}$$

References

[1] L.G. Nallim, R.O. Grossi, A general algorithm for the study of the dynamical behaviour of beams, *Applied Acoustics* 57 (4) (1999) 345–356.

[2] N.M. Auciello, A. Ercolano, A general solution for dynamic response of axially loaded non-uniform Timoshenko beams, *International Journal of Solids and Structures* 41 (18–19) (2004) 4861–4874.

[3] D. Zhou, Free vibration of multi-span Timoshenko beams using static Timoshenko beam functions, *Journal of Sound and Vibration* 241 (4) (2001) 725–734.

[4] N.G. Stephen, On Southwell's and a novel Dunkerley's method, *Journal of Sound and Vibration* 181 (1) (1995) 179–184.

[5] R.O. Grossi, C.M. Albarracin, Some observations on the application of the Rayleigh–Ritz method, *Applied Acoustics* 62 (10) (2001) 1171–1182.

[6] R. Greif, S.C. Mittendorf, Structural vibrations and Fourier series, *Journal of Sound and Vibration* 48 (1) (1976) 113–122.

[7] S. Singhvi, R.K. Kapania, Comparison of simple and Chebychev polynomials in Rayleigh–Ritz analysis, *Journal of Engineering Mechanics* 120 (10) (1994) 2126–2135.

[8] L. Meirovitch, *Principles and Techniques of Vibrations*, Prentice-Hall, Inc., New Jersey, 1997.

[9] A.S. Yigit, A.P. Christoforou, Coupled axial and transverse vibrations of oilwell drillstrings, *Journal of Sound and Vibration* 195 (4) (1996) 617–627.

[10] E. Barbieri, U. Ozguner, Unconstrained and constrained mode expansions for a flexible slewing link, *Journal of Dynamic Systems, Measurement and Control, Transactions ASME* 110 (4) (1988) 416–421.

[11] W.D. Zhu, C.D.J. Mote, Dynamic modeling and optimal control of rotating Euler–Bernoulli beams, *Proceedings of the American Control Conference*, Vol. 5, Albuquerque, NM, USA, June 4–6, 1997, pp. 3110–3114.

[12] M. Gurgoze, S. Yuksel, Transverse vibrations of a flexible beam sliding through a prismatic joint, *Journal of Sound and Vibration* 223 (3) (1999) 467–482.

[13] H.H. Yoo, S.H. Shin, Vibration analysis of rotating cantilever beams, *Journal of Sound and Vibration* 212 (5) (1998) 807–808.

[14] M.L. Chen, Y.S. Liao, Vibrations of pretwisted spinning beams under axial compressive loads with elastic constraints, *Journal of Sound and Vibration* 147 (3) (1991) 497–513.

[15] J.T.S. Wang, Dynamic analysis of cantilever beams, American Society of Mechanical Engineers, Paper 79-PVP-78, 1979, pp. 1–9.

[16] N. Popplewell, D. Chang, Free vibrations of a stepped, spinning Timoshenko beam, *Journal of Sound and Vibration* 203 (4) (1997) 717–722.

[17] J.S. Jensen, D.M. Tcherniak, J.J. Thomsen, Stiffening effects of high-frequency excitation: experiments for an axially loaded beam, *Journal of Applied Mechanics, Transactions ASME* 67 (2) (2000) 397–402.

[18] R.K. Jha, R.G. Parker, Spatial discretization of axially moving media vibration problems, *Journal of Vibration and Acoustics, Transactions of the ASME* 122 (3) (2000) 290–294.

[19] P.Z. Bar-Yoseph, D. Fisher, O. Gottlieb, Spectral element methods for nonlinear spatio-temporal dynamics of an Euler–Bernoulli beam, *Computational Mechanics* 19 (2) (1996) 136–151.
[20] J.S. Rao, The fundamental flexural vibration of a cantilever beam of rectangular cross section with uniform taper, *Aeronautical Quarterly* 16 (1965) 139–144.
[21] C. Kameswara Rao, S. Mirza, Torsional vibrations and buckling of thin-walled beams on elastic foundation, *Thin-Walled Structures* 7 (1) (1989) 73–82.
[22] J.R. Banerjee, F.W. Williams, Exact dynamic stiffness matrix for composite Timoshenko beams with applications, *Journal of Sound and Vibration* 194 (4) (1996) 573–585.
[23] J.R. Banerjee, Dynamic stiffness formulation and its application for a combined beam and a two degree-of-freedom system, *Journal of Vibration and Acoustics, Transactions of the ASME* 125 (3) (2003) 351–358.
[24] J.R. Banerjee, H. Su, D.R. Jackson, Free vibration of rotating tapered beams using the dynamic stiffness method, *Journal of Sound and Vibration* 298 (4–5) (2006) 1034–1054.
[25] M. Eisenberger, An exact high order beam element, *Computers and Structures* 81 (3) (2003) 147–152.
[26] M. Eisenberger, Dynamic stiffness matrix for variable cross-section Timoshenko beams, *Communications in Numerical Methods in Engineering* 11 (6) (1995) 507–513.
[27] A.Y.T. Leung, Dynamic stiffness method for exponentially varying harmonic excitation of continuous systems, *Journal of Sound and Vibration* 98 (3) (1985) 337–347.
[28] J.R. Banerjee, Dynamic stiffness formulation for structural elements: a general approach, *Computers and Structures* 63 (1) (1997) 101–103.
[29] W.H. Wittrick, F.W. Williams, A general algorithm for computing natural frequencies of elastic structures, *Quarterly Journal of Mechanics and Applied Mathematics* 24 (1971) 263–284.
[30] J.R. Banerjee, F.W. Williams, Coupled bending-torsional dynamic stiffness matrix of an axially loaded Timoshenko beam element, *International Journal of Solids and Structures* 31 (6) (1994) 749–762.
[31] J.R. Banerjee, S.A. Fisher, Coupled bending-torsional dynamic stiffness matrix for axially loaded beam elements, *International Journal for Numerical Methods in Engineering* 33 (4) (1992) 739–751.
[32] J.R. Banerjee, Explicit modal analysis of an axially loaded Timoshenko beam with bending–torsion coupling, *Journal of Applied Mechanics, Transactions of the ASME* 67 (2) (2000) 307–313.
[33] J.R. Banerjee, H. Su, Development of a dynamic stiffness matrix for free vibration analysis of spinning beams, *Computers and Structures* 82 (23–26) (2004) 2189–2197.
[34] J.R. Banerjee, H. Su, Dynamic stiffness formulation and free vibration analysis of a spinning composite beam, *Computers and Structures* 84 (19–20) (2006) 1208–1214.
[35] J.R. Banerjee, Development of an exact dynamic stiffness matrix for free vibration analysis of a twisted Timoshenko beam, *Journal of Sound and Vibration* 270 (1–2) (2004) 379–401.
[36] P. Ruta, Application of Chebyshev series to solution of non-prismatic beam vibration problems, *Journal of Sound and Vibration* 227 (2) (1999) 449–467.
[37] P. Ruta, The vibration of a nonprismatic beam on an inertial elastic half-plane, *Journal of Sound and Vibration* 275 (3–5) (2004) 533–556.
[38] P. Ruta, The application of Chebyshev polynomials to the solution of the nonprismatic Timoshenko beam vibration problem, *Journal of Sound and Vibration* 296 (1–2) (2006) 243–263.
[39] J. Lee, W.W. Schultz, Eigenvalue analysis of Timoshenko beams and axisymmetric Mindlin plates by the pseudospectral method, *Journal of Sound and Vibration* 269 (3–5) (2004) 609–621.
[40] A.E. Lovejoy, R.K. Kapania, Free vibration of thick generally laminated quadrilateral plates with point supports, *Collection of Technical Papers—AIAA/ASME/ASCE/AHS/ASC Structures, Structural Dynamics and Materials Conference*, Salt Lake City, UT, USA, April 15–17, 1996, pp. 248–258.
[41] D. Gottlieb, S.A. Orszag, *Numerical Analysis of Spectral Methods, Theory and Applications*, SIAM-CBMS, Philadelphia, PA, 1977.
[42] P.J. Boyd, *Chebyshev and Fourier Spectral Methods*, second ed., Dover Publications, New York, 2001.
[43] C. Canuto, M.Y. Hussaini, A. Quarteroni, T.A. Zang, *Spectral Methods in Fluid Dynamics*, first ed., Springer, Berlin, 1993.
[44] W.H. Press, S.A. Teukolsky, W.T. Vetterling, *Numerical Recipes*, second ed., Cambridge University Press, Cambridge, UK, 2002.
[45] S. Filiz, O.B. Ozdoganlar, L.A. Romero, An analytical model of micro-endmill dynamics, *Journal of Vibration and Controls* 14 (8) (2008) 1125–1150.
[46] S. Filiz, O.B. Ozdoganlar, Micro-endmill dynamics including the actual fluted geometry and setup errors - Part 1: Model development and numerical solution, Journal of Manufacturing Science and Engineering 130 (3) (2008) 031119-1-10.
[47] M.I. McEwan, J.R. Wright, J.E. Cooper, A.Y.T. Leung, A combined modal/finite element analysis technique for the dynamic response of a non-linear beam to harmonic excitation, *Journal of Sound and Vibration* 243 (4) (2001) 601–624.
[48] S. Woinowski-Krieger, The effect of an axial force on the vibration of hinged bars, *Journal of Applied Mechanics* 17 (1950) 35–36.
[49] H.R. Srirangarajan, Non-linear free vibration of uniform beams, *Journal of Sound and Vibration* 175 (3) (1994) 425–427.
[50] D.A. Evensen, Nonlinear vibrations of beam with various boundary conditions, *AIAA Journal* 6 (2) (1968) 370–372.
[51] G. Singh, A.K. Sharma, G. Venkateswara Rao, Large-amplitude free vibration of beams—a discussion on various formulations and assumptions, *Journal of Sound and Vibration* 142 (1) (1990) 77–85.
[52] A.V. Srinivasan, Large amplitude free oscillations of beams and plates, *AIAA Journal* 3 (1965) 1951–1953.

[53] G. Singh, G. Venkateswara Rao, N.G.R. Iyengar, Reinvestigation of large-amplitude free vibrations of beams using finite elements, *Journal of Sound and Vibration* 143 (2) (1990) 351–355.
[54] C. Mei, Nonlinear vibrations of beam by matrix displacement method, *AIAA Journal* 10 (3) (1972) 355–357.
[55] O.B. Ozdoganlar, B.D. Hansche, T.G. Carne, Experimental modal analysis for microelectromechanical systems, *Experimental Mechanics* 45 (6) (2005) 498–506.
[56] E.S. Hung, S.D. Senturia, Generating efficient dynamical models for microelectromechanical systems from a few finite-element simulation runs, *Journal of Microelectromechanical Systems* 8 (3) (1999) 280–289.